Constraining porewater chemistry in a 250 m thick argillaceous rock se-quence

Paul Wersin, Martin Mazurek, Thomas Gimmi, Daniel Rufer, Catherine Lerouge, Daniel Traber

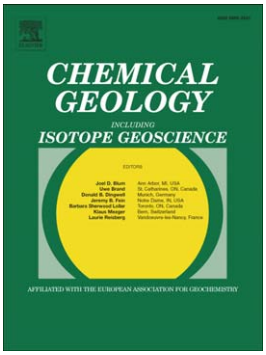

Constraining porewater chemistry in a 250 m thick argillaceous rock sequence

Paul Wersin, Martin Mazurek, Urs K. Mäder, Thomas Gimmi, Daniel Rufer, Catherine Lerouge, Daniel Traber

PII: S0009-2541(16)30171-1
DOI: doi: 10.1016/j.chemgeo.2016.04.006
Reference: CHEMGE 17900

To appear in: *Chemical Geology*

Received date: 18 December 2015
Revised date: 5 April 2016
Accepted date: 7 April 2016

Please cite this article as: Wersin, Paul, Mazurek, Martin, Mäder, Urs K., Gimmi, Thomas, Rufer, Daniel, Lerouge, Catherine, Traber, Daniel, Constraining porewater chemistry in a 250 m thick argillaceous rock sequence, *Chemical Geology* (2016), doi: 10.1016/j.chemgeo.2016.04.006

Constraining porewater chemistry in a 250 m thick argillaceous rock sequence

Paul Wersin[1*], Martin Mazurek[1], Urs K. Mäder[1], Thomas Gimmi[1], Daniel Rufer[1], Catherine Lerouge[2] and Daniel Traber[3]

[1] Rock-Water Interaction, Institute of Geological Sciences, University of Bern, Baltzerstrasse 1+3, 3012 Bern, Switzerland

[2] BRGM-ISTO-UMR 7327, 3 av. C. Guillemin, B.P. 36009, Orléans, 45060, France

[3] NAGRA, Hardstrasse 73, 5430 Wettingen, Switzerland

***** corresponding author: email: paul.wersin@geo.unibe.ch, phone: +41 31 631 4537 fax: +41 31 631 4843

Table of contents

Abstract

The geochemistry of an argillaceous rock sequence from a deep borehole in NE-Switzerland was investigated. The focus was to constrain the porewater chemistry in low permeability Jurassic rocks comprising the Liassic, the Opalinus Clay formation, the 'Brown Dogger' unit and the Effingen Member (Malm). A multi-method approach including mineralogical analysis, aqueous and Ni-ethylenediamine extraction, squeezing tests and pCO_2 measurements as well as geochemical modelling was applied for this purpose. A consistent dataset was obtained with regard to the main solutes in the porewaters. A fairly constant anion-accessible porosity of ~50% of the total porosity was deduced for all analysed samples which displayed variable clay-mineral contents. Sulphate concentrations were shown to be constrained by a sulphate-bearing phase, presumably by celestite or a Sr-Ba sulphate. Application of a simple equilibrium model, including cation exchange reactions, calcite and celestite equilibrium showed good agreement with squeezing data, indicating the suitability of the modelling approach to simulate porewater chemistry in the studied argillaceous rocks. The modelling highlighted the importance of correct determination of the exchangeable cation population. The analysis corroborates that squeezing of the studied rocks is a viable and efficient way to sample porewater.

Keywords: argillaceous rocks, porewater chemistry, anion exclusion, modelling

1. Introduction

Argillaceous rock formations are generally characterised by low hydraulic conductivity and thus solute transport is governed by diffusion. Because of this property, they may act as natural barriers, and thus serve as caprocks for oil and gas reservoirs or as host rocks for radioactive waste repositories. It is important to constrain the porewater chemistry in such low permeability clayrocks because it affects the transport of solutes or, more specifically, of contaminants such as radionuclides. The intimate association of water with the nanoporous clayrock, however, makes the sampling and characterisation of porewater chemistry a difficult task (Sacchi et al. 2000). Thus, virtually every extraction method may create disturbances and alter the in-situ porewater chemistry.

Presumably because of the aforementioned experimental difficulties, there are comparatively few published studies of porewater chemistry in clayrocks. Most of these have been focussed on the investigation of porewaters of clay-rich formations proposed as host rocks for geological radioactive waste disposal. In a pioneer synthesis study, Pearson et al. (2003) compiled data from different experimental extraction techniques and seepage waters from the Opalinus Clay formation in the Mont Terri underground rock laboratory (URL) in Switzerland. Based on these data, the authors proposed a fairly simple chemical equilibrium modelling approach for describing porewater compositions. The same type of approach was initially applied to define porewater chemistry for the Callovo-Oxfordian formation at the URL at the Bure site in France (Gaucher et al. 2006) and was later refined (Appelo et al. 2008, Gaucher et al. 2009). The sensitivity of different equilibrium-type models was evaluated for Opalinus Clay porewaters (Pearson et al. 2011). Earlier geochemical characterisation and modelling of porewaters in the weakly consolidated Boom Clay at the URL at Mol (Belgium) was reported in Beaucaire et al. (2000). More recently, characterisation and modelling

studies were conducted on the strongly consolidated Toarcian/Domerian clayrock at the Tournemire URL site in France (Beaucaire et al. 2008; Tremosa et al. 2012).

A systematic finding in these and other (e.g. Mazurek et al. 2012) studies was the effect of anion exclusion arising from the negative structural charge of smectite and illite, which are abundant in such argillaceous rocks. Considering anion exclusion, consistent profiles for chloride could be obtained by applying aqueous extraction, squeezing and water sampling in boreholes (e.g. Pearson et al. 2003, Mazurek et al. 2012).The derived anion-accessible porosity was in many instances found to be around 50% of the total porosity (Pearson et al. 2003; Gaucher et al. 2006; 2009; Mazurek et al. 2011) for different argilleaceous rocks with variable clay-mineral content.

A further finding in all studied clayrocks was the important role of cation exchange in constraining major cations, such as Na^+, Ca^{2+}, Mg^{2+} and K^+. Using a "classical" cation exchange model calibrated for smectite and illite data, fairly consistent results could be obtained for different clayrock samples of Callovo-Oxfordian shale and Opalinus Clay (Tournassat et al. 2007; 2009; Gaucher et al. 2009; Pearson et al. 2011). Differences encountered between modelled and measured data seemed often to be related to methodological uncertainties in cation exchange capacity (CEC) and exchangeable cations analyses (e.g. Tournassat et al. 2009).

Mineral equilibria reactions pose a further constraint to solute chemistry of clayrocks, which contain variable types and contents of carbonates. Calcite equilibrium has been invoked in all modelling studies mentioned above. Dolomite, siderite and, in the case of Opalinus Clay, ankerite are also encountered, but whether these phases are in equilibrium with the pore fluid is less obvious (Tournassat et al. 2008; Gaucher et al. 2009; Pearson et al. 2011). Pyrite is generally the main sulphur-bearing phase in argillaceous rocks. High sulphate levels found in aqueous extracts and squeezed samples may arise from pyrite oxidation during sampling, storage and/or porewater extraction procedure (De Craen et al. 2006; Gaucher et al. 2009). The latter authors showed for aqueous extraction data from carefully stored Callovo-Oxfordian shale cores that sulphate in the porewater was likely controlled by celestite, the presence of which as infill in bioclasts and veins was later confirmed (Lerouge et al. 2011). For Opalinus Clay porewater, control of sulphate remains ambiguous. Fixed SO_4/Cl at seawater ratio was considered in earlier work based on aqueous extraction data (Pearson et al. 2003), but the possibility of control by celestite has been discussed (Pearson et al. 2011). In a recent petrographic study of Opalinus Clay cores of the deep borehole in Benken (NE Switzerland), diagenetically formed Sr-Ba sulphate as well as celestite as infill in faults was observed (Lerouge et al. 2014).

This contribution documents the geochemical analysis of a 250 m thick, strongly consolidated argillaceous rock sequence in the Swiss Molasse Basin comprising the Opalinus Clay formation and its confining units (Nagra 2002). The data were obtained from carefully conditioned drill cores of a deep geothermal borehole. A multi-method approach was applied including petrophysical measurements, X-ray diffraction (XRD), scanning electron microscopy (SEM), aqueous extraction, squeezing, analyses of CEC and exchangeable cations and CO_2 partial pressure measurements. The objective was to constrain the porewater chemistry, thus to extend the geochemical database for Opalinus Clay as host rock for a geological waste repository and to acquire data on the underlying and overlying argillaceous units. The latter display more variability in terms of clay-mineral

contents, particularly the overlying unit termed ‘Brown Dogger’. The specific goals were (i) to test the robustness of the equilibrium modelling approach for describing porewater compositions in the analysed rock sequence, (ii) to determine anion-accessible porosities and their relation to mineralogy based on chloride data, and (iii) to evaluate processes constraining sulphate in the porewater.

2. Geological setting

A deep geothermal borehole was drilled to a final depth of 1508 m at Schlattingen (Thurgau, Switzerland) at the Eastern border of the Swiss Molasse Basin in the year 2011. The primary objective of the campaign was to explore the Triassic aquifers (Muschelkalk and Buntsandstein) and the crystalline basement for their suitability as a geothermal resource. A further objective was to extend the geological and geochemical database of the Opalinus Clay and the adjacent argillaceous units. The Schlattingen borehole is located 9 km ENE from the well-investigated deep borehole at Benken (Nagra 2002, Gimmi et al. 2007) and is in the vicinity of a potential siting area for a high-level radioactive waste repository (Nagra 2014).

As shown in Fig. 1, the borehole penetrated through Mesozoic and Permian sedimentary rocks dipping at ~4° to the SE into the crystalline basement (Variscan gneisses). The Mesozoic is unconformably overlain by Tertiary and Quaternary deposits at 491 m depth (not shown). The basin was subjected to a complex burial and uplift history (Mazurek et al. 2006). For the Benken borehole, a maximum burial of 1650 m and a maximum temperature of 85 °C were obtained for the Opalinus Clay, and these values are considered to be representative for Schlattingen as well. Since maximum burial at 5–10 Ma, the sequence was uplifted by about 1 km, leading to overconsolidation.

The studied Jurassic argillaceous rock sequence can be roughly divided into four units (Fig. 1): The top (~25 m thick) corresponds to the Effingen Member (lower Malm) and is made up of silty to sandy calcareous marls to limestones. The underlying unit (~77 m thick), termed ‘Brown Dogger’, exhibits rather variable lithology. It consists predominantly of clayrocks and marls but also includes sandy-calcareous beds. The third unit is the ~120 m thick Opalinus Clay (Aalenian), consisting of fairly homogeneous silty to fine sandy clayrocks. The lowest ~53 m thick unit termed Lias is also rather clay-rich and is mainly made up of a variable sequence of marls and clayrocks. Based on analogy with the Benken borehole, it can be expected that the clay-rich sequence is bounded by the underlying aquifer in the upper middle Keuper and the overlying Malm aquifer.

The evolution and the relationships of diagenetically-formed minerals in Opalinus Clay have have been studied by Wersin et al. (2013) and Lerouge et al. (2014) on cores obtained from the Schlattingen and Benken boreholes, respectively. Sediment deposition occurred in a shallow marine environment. Early diagenesis, i.e. processes near the interface between water and the unconsolidated sediment, had the most significant impact. Minerals precipitated include pyrite, siderite and minor calcite, dolomite and ankerite. The most significant imprint of subsequent burial diagenesis is the cementation of silty horizons by calcite, whereas clay-rich beds are essentially uncemented. Also, in this phase, maturation of organic matter and limited recrystallization of clay minerals occurred (Mazurek et al. 2006).The last stage of mineralisation is related to normal to strike-slip faulting – e.g.

recorded in the Schlattingen core –, linked to Miocene movements in the adjacent Hegau-Bodensee graben. This faulting led to local fluid circulation and the precipitation of calcite-celestite veins. Solid solutions of celestite and barite also occur as trace constituents disseminated in the rock matrix. Their age is difficult to constrain accurately on the basis of textural relationships. It is likely that precipitation occurred both during early diagenesis (fillings of residual pore space) and during burial diagenesis, (overgrowths of pyrite and siderite). The likely source of Sr is the dissolution of aragonite in fossil shells. Given the fact that the original aragonitic ammonite shells are locally still preserved in Opalinus Clay (Seilacher et al. 1976), this reservoir of Sr has been available over the entire evolution of the formation.

It is evident that the marine pore water originally trapped in the sediment was substantially modified during early diagenesis (e.g. establishment of reducing conditions, removal of SO_4^{2-} by microbially mediated pyrite precipitation). The later evolution of pore-water composition is difficult to constrain in detail. It was controlled by equilibria with the clastic and diagenetic minerals present in the sequence and, importantly, by diffusive exchange with over- and underlying units with higher permeability (Fig. 1). Since the regional uplift in the late Cretaceous, the area has been exposed to continental conditions (with one marine episode in the Burdigalian recorded in the Upper Marine Molasse). This led to substantial erosion and the karstification of the Malm limestones, which constitute the upper hydraulic and geochemical boundary of the low-permeability sequence today. Three Triassic aquifers underlie the sequence (Fig. 1), with one in the Keuper sandstones and dolomites being the closest one. Given the abundance of evaporites in the Triassic, it is likely that sulphate present in the low-permeability sequence today partially diffused in from the footwall. The last ca. 1 Ma of the pore-water evolution is detailed in Gimmi et al. (2007) for Benken. At this time, the exhumation and activation of the Keuper aquifers led to a drop in salinity and therefore to the development of a diffusion profile in the pore waters of the low-permeability sequence.

The Keuper aquifer has pronounced lateral lithological heterogeneity, which is also manifested in the lateral variability in hydraulic conductivity. The overlying Malm aquifer consists of a 200−300 m thick sequence of karstified limestones with highly variable hydraulic conductivities (Nagra 2002), but the local hydraulic conditions at the Schlattingen site are not known. The hydraulic conductivity of the undisturbed rock-matrix of the clay-rich sequence is known to be extremely low (Nagra 2002, Nagra 2014). For the Opalinus Clay, reference values are $2 \cdot 10^{-14}$ m/s and $1 \cdot 10^{-13}$ m/s normal and parallel to bedding, respectively. Therefore, the dominating transport process for solutes in this formation is diffusion (Gimmi et al. 2007, Mazurek et al. 2011). A temperature of 45° C was measured in a water sample extracted from the Schlattingen borehole from a section at 799-833 m depth (Nagra, unpubl. data).

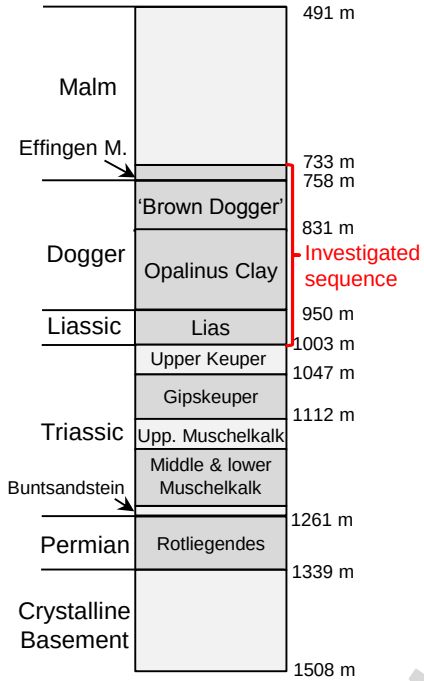

Fig. 1 Simplified geological profile encountered in the Schlattingen borehole (section above 491 m depth not shown). White sections contain permeable strata, grey shaded units represent aquitards

3. Experimental methods

3.1 Sampling of drillcores

The sampling and analytical procedures used for the drillcores (diameter 10 cm) are extensively described in Wersin et al. (2013). Here we briefly describe the procedures relevant to the porewater data.

The emphasis for the so-called standard samples was to provide coverage of the whole profile at largely even spacing between samples with a higher frequency toward the expected aquifers. Standard samples of ~25 cm length were taken approximately every 5 m. Given the lithological heterogeneity and natural or induced fracturing, some deviation from the strictly even spacing had to be accepted. From the 53 standard samples 30 were processed for subsequent analyses, and the remaining were kept as backup material. Table SI-1 in the Supplementary Information (S.I.) lists all standard samples together with their depth location and applied analytical methods. These include density and porosity measurements, XRD analysis, aqueous extraction (all samples), and measurement of cation exchange parameters (selected samples). Furthermore, core samples were taken for porewater squeezing and microscopic analysis. These samples are listed together with their location and applied analytical methods in Table SI-2 (S.I.).

The goal of the sampling procedure of the drillcores was to ensure preservation of in-situ conditions of the porewater in the saturated state and hence to minimise (i) drilling-induced contamination, (ii) desaturation, and (iii) oxidation of the cores. Core surfaces were carefully cleaned with groundwater available from the site. After geological survey and photographic documentation, the cores were protected from the atmosphere. When multiple samples had to be processed, they were preserved in temporary plastic bags evacuated by vacuum

sealing. These samples and those without the temporary protection were put into a thick plastic-coated aluminium bag, which was evacuated and heat-sealed. All samples were additionally sealed inside a robust plastic bag for mechanical protection of the Al-bag which served as the main gas barrier. On-site, samples were stored at approximately 10° C in coolers containing ice packs until they could be transported to the laboratory at the University of Bern, where they were stored at 4° C in a refrigerated room.

For the CO_2 samples, core sections were trimmed by dry cutting to a square-shaped central section to remove the potentially partly degassed and drill fluid/cleaning water contaminated core rim. All cut surfaces were brushed off to remove rock powder from the sawing process. The samples were placed into sample containers equipped with pressure gauges with 10 mbar resolution. Helium gas (99% purity) was used as the flushing and conditioning gas.

3.2 Analytical procedures

3.2.1 Mineralogy

The mineral compositions were determined by X-ray diffractometry using a Philips PW3710 diffractometer. Rock material from the rim of the drillcores was ground in a ring mill to a grain size of less than 2 µm, mounted on a sample holder, non-orientated with a stamp, and scanned with Cu Kα radiation from 2° to 70° 2θ angle. The contents of quartz, feldspars and carbonates (calcite, dolomite, siderite) were quantified by standardisation utilising the diffraction peak-intensity ratio of the mineral to that of an internal LiF-standard. The relative error of such determinations is about ± 5%. The standardisation used is valid for individual mineral contents up to approximately 50 wt%. In limestones, the contents of calcite or dolomite often exceed 50 wt%. The relative contents of the carbonate minerals derived from the XRD peak intensities were calibrated using the total inorganic carbon content measured by infrared (IR) spectroscopy (see below). The pyrite content was similarly calculated from the total sulphur concentration measured by IR spectroscopy assuming that pyrite is the dominating sulphur-bearing mineral phase. Sheet silicates, which are mainly clay minerals, were estimated by difference with the percentages of all other phases.

For the identification of individual clay-mineral phases, the <2 µm fraction was separated by sedimentation, and oriented samples were prepared. Air-dried, glycolated and heated samples were used for X-ray diffractometry (2 °/min from 2 to 40 ° 2θ angle using Cu Kα radiation). The relative ratios of the individual clay minerals were determined using the ARQUANT model (Blanc et al. 2006). This Excel-based tool compares the X-ray pattern of glycolated samples with patterns from a standard library, which contains a large number of patterns for clay minerals and other sheet silicates. The relative amounts of clay-mineral species were calculated using the NEWMOD code (Reynolds 1985). A more detailed documentation is provided in Wersin et al. (2013).

The concentrations of total carbon (C_{tot}), inorganic carbon (C_{inorg}) and total sulphur (S_{tot}) were determined with G4 ICARUS Carbon/Sulfur Analyser with infrared detection (Bruker Corporation). The detection limits are around 0.1 wt% for S_{tot}, C_{tot} and C_{inorg}.

Thin sections were made from six drillcore samples (Table SI-2, S.I.) which contained silty-sandy layers. The goal was to identify diagenetic minerals and their textural relationships. The sections were studied with a conventional optical polarising microscope under transmitted and reflected light. Furthermore, a scanning electron microscopic (SEM) analysis including energy dispersive x-ray (EDX) measurements of selected diagenetic minerals was

conducted. Additionally, thin sections were made from 18 vein samples taken from various parts of the stratigraphic column (Table SI-2, S.I.). They were prepared the same way as those used for diagenetic analysis. The sections were studied with a conventional optical polarising microscope under transmitted and reflected light.

3.2.2 Petrophysical measurements

The water content of the preserved core samples (relative to the wet mass) was obtained by gravimetric determination of water loss. Water-loss was measured by drying sample aliquots of between 140 to 220 g at 105° C to constant weight. The analytical uncertainty was determined from the standard deviation of measurements of four subsamples. The water-loss porosity or volumetric moisture content of a rock sample (ϕ_{WL}) is the ratio of its connected water-filled pore volume to its total volume and is obtained according to:

$$\phi_{WL} = \frac{w_w \cdot \rho_g}{w_w \cdot \rho_g + (1 - w_w) \cdot \rho_{pw}} \quad (1)$$

where w_w is the water content of the rock relative to its wet mass (water content in the following), ρ_{pw} = density of the porewater, and ρ_g = grain density of the rock. For the porewater, a density of 1.00 g/cm^3 was assumed throughout. This is justified by the relatively low salinities obtained from the Schlattingen borehole, which are below that of seawater. The analytical error for the water-loss porosity was estimated from first order error propagation. Grain density (ρ_g) was measured in quadruplicate by kerosene-pycnometry (Mazurek et al. 2012). The error including possible small-scale variability was determined from the standard deviation of the grain density from the 4 subsamples.

3.2.3 Aqueous extracts

Extraction conditions were chosen to attain equilibrium with calcite by extracting over 48 hours and to suppress sulphide mineral oxidation by working in an oxygen-free atmosphere. The amount of ground and dried rock material varied between about 4 g and 30 g for the different S/L weight ratios of 0.1, 0.25, 0.5 and 1 (in units of g rock per g solution). Duplicate extracts were prepared and analysed from aliquots of each sample. The ground rock material was placed in polypropylene tubes filled with an appropriate mass of degassed, oxygen- and CO_2-free water that was prepared in the glovebox by boiling and N_2-bubbling over 30 minutes. Each suspension was shaken end-over-end for 48 hours in a polypropylene tube. The tubes were then removed from the glovebox and centrifuged for 1 hour. Subsequently, the supernatant solution was filtrated using 0.45µm millipore filters and immediately analysed for pH and alkalinity with a Metrohm Titrino DMP 785 system. Major anions (F^-, Cl^-, Br^-, NO_3^-, SO_4^{2-}) and cations (Na^+, K^+, Ca^{2+}, Mg^{2+}, NH_4^+, and Sr^{2+}) were analysed simultaneously in the remaining solutions by ion chromatography using a Metrohm ProfIC AnCat MCS IC system with automated 5µl and 50µl injection loops. The detection limit of this technique is 0.016 mg/l for anions and 0.1 mg/l for cations with an analytical error of ± 5% based on multiple measurements of standard solutions. Concentrations of K^+, Mg^{2+} and Sr^{2+} that were close to or below the detection limit in the ion chromatographic method were re-analysed using a Varian 710 ES ICP-OES system with a detection limit of 0.01 mg/l and an analytical error of ± 10% for these elements. Anion concentrations were analysed using a Metrohm ASupp5-150 separation column, which is not suited for the quantitative separation of low-molecular weight organic acids so that such substances were not quantified, but only qualitatively identified. Larger concentrations of low-molecular organic

acids were indicated in a few samples. For these samples, some interference of low-molecular organic acids with the F^- peak occurred, which results in a larger uncertainty of about 10–20% for the F^- concentration in these few samples.

3.2.4 Cation exchange parameters

Cation exchange properties were studied using the nickel ethylenediamine (Ni-en) method following the experimental protocol elaborated by Baeyens and Bradbury (1994) and Bradbury and Baeyens (1997/98). Ni-en extractions were performed on the pulped material at 4 different S/L ratios for six samples. The amount of pulped rock material varied between about 4 and 30 g for the different S/L weight ratios of 0.1, 0.25, 0.5 and 1.0. The Ni-en solution was prepared by adding ethylenediamine to a $Ni(NO_3)_2$ solution to obtain a 0.1 molar Ni-en stock solution. According to the protocol of Bradbury & Baeyens (1997/1998) the Ni-en content of the added solution is adjusted to approximately twice the expected CEC value, thus diluting the stock solution according to the S/L ratio. For the Schlattingen samples, a simplified approach was adopted instead and 0.1 molar Ni-en solution was added irrespective of the solid concentration using degassed, oxygen- and CO_2-free water that was prepared in the glovebox by boiling and N_2-bubbling for 30 minutes. As a result, slightly larger (high S/L) or clearly larger (low S/L) amounts compared to two times the expected CEC were added. This probably led to enhanced dissolution of carbonates, as discussed in section 4.4. The pH of the Ni-en solution was buffered to 8.0−8.2 by adding HNO_3 TitrisolTM solution. Each sample was shaken end-over-end for 7 days in a polypropylene tube in order to equilibrate the extract solution with calcite and dolomite. After phase separation by centrifugation, the supernatant leach solution was removed using a syringe and was filtered to <0.45 µm. Analyses of major cations (Na^+, K^+, Ca^{2+}, Mg^{2+} and Sr^{2+}) and Ni^{2+} were carried out using Varian Spectra 300 atomic absorption spectrometer (AAS). The analytical error of these measurements is less than ±5% based on multiple measurements of standard solutions and based on control measurements conducted with the Varian 710 ES ICP-OES system of the same solutions. The cumulative error of the entire procedure (*i.e.* extraction and analysis) is approximately 10 %. The cation exchange capacity (CEC) was derived from the Ni consumption, *i.e.* the difference between the Ni concentration in the initial and the final extract solution.

3.2.5 Squeezing tests

Squeezing tests were conducted at the Central Research Institute of Electric Power Industry (CRIEPI, Japan) at pressures of 200, 300, 400 and 500 MPa. These tests are described in detail in Mazurek et al. (2015). Here only the tests at the lowest squeezing pressure of 200 MPa, thought to represent in-situ conditions most closely, are reported. The cylindrical sample chamber is connected to fiber glass filters, where pore water was collected in syringes. Pressure was exerted by a piston located above the sample chamber. The total dead volume of the system was less than 0.25 mL. The drillcore samples were dry cut to polygonal prisms to the size and shape needed for the squeezing cell, so that at least the outermost 2.5 cm of the core were removed. Porewaters obtained at each pressure step were collected and stored cool in 4 mL plastic bottles and then sent to RWI, University of Bern, for chemical analysis. Squeezed samples were subsequently subjected to aqueous extraction. About 30 g of dried and ground rock material were extracted at a S/L ratio of 1 under atmospheric conditions. Each suspension was shaken end-over-end for 48 hours in a polypropylene tube and then centrifuged for 1 hour. The supernatant solution was filtrated using 0.45 µm millipore filters.

Squeezed waters and aqueous extracts were analysed for major ions by ion chromatography using a Metrohm ProfIC AnCat MCS IC system Metrohm ASupp5-150 separation column (see aqueous extraction method). Fluoride and, to a lesser extent, nitrate concentrations turned out be unrealistically high and were probably affected by contamination of the filter equipment.

3.2.6 CO_2 partial pressure measurements

In the porewater of carbonate-bearing clayrocks, the partial pressure of CO_2 is linked to pH, thus determining the pCO_2 is a way to evaluate the pH of porewater. However, the low permeability of clayrocks makes it difficult to measure in-situ partial pressures of gases (CO_2, alkanes and others) due to degassing (Lassin et al. 2000). A methodology was developed to collect CO_2, alkanes and other gas liberated from cores, using specifically-designed outgassing cells (Lassin et al. 2000; Girard et al. 2005; Gaucher et al. 2010). Core samples were conditioned in a gas cell under an inert gas atmosphere (here He) until the outgassed pCO_2 reached a plateau. This partial pressure of CO2 corresponds to a pseudo-equilibrium between the porewater and the minerals (Gaucher et al. 2010).

The gas cells were stored in a climatised room at a temperature of 20−21° C. The equilibration time between the core and the gas ranged from 2 months to 1 year (Gaucher et al. 2010). Gas pressure and temperature were monitored and chemical gas analyses were periodically performed on a Varian star 3400 CX gas chromatograph. The concentrations of CO_2 and alkanes were determined at a known total gas pressure, measured in-line. O_2 and N_2 were analysed in a first step using a calibration with O_2 and N_2 from air. CO_2 and alkanes were analysed in a second step using a calibration performed with a CO_2-CH_4 standard and a standard containing a mixture of different alkanes. The concentrations of CO_2 and alkanes were converted into gas partial pressures (P_{gas} in mbar), as $P_{gas} = C_{gas} \times P_{tot} / 100$, where C_{gas} is the gas concentration (vol%) and P_{tot} is the total pressure in the gas cell.

3.3 Modelling procedures for the in-situ porewater composition

A chemical equilibrium model for describing in-situ porewater compositions was applied based upon the approach adopted by Pearson et al. (2003; 2011) for Opalinus Clay and Gaucher et al. (2009) for the Callovo-Oxfordian shale. The modelling follows the Gibbs' phase rule, in which - at constant temperature and pressure - the number of free solute concentrations is fixed by the equal number of phases with which the porewater solution is in equilibrium.

The concentrations of solutes which are not controlled by water-rock reactions, such as Cl^- and Br^-, need to be obtained from measurements. In this work, Cl^- concentrations were derived from the Cl^- inventory in the rock (Br^- was not included in the model) and accounting for the anion-accessible porosity fraction, as discussed in section 5.1. The other solute concentrations considered in the model are constrained by two types of reactions: (i) mineral and gas dissolution and (ii) cation exchange reactions.

Cation exchange equilibrium is expressed by considering the selectivity of exchangeable cations (K^+, Ca^{2+}, Mg^{2+}, Sr^{2+}) relative to Na:

$$K^{Na^+/Me^{z+}} = \frac{a_{Na^+}^{z}}{a_{Me^{z+}}} \times \frac{a_{MeX_z}}{a_{NaX}^{z}} \quad (2)$$

where $K^{Na^+/Me^{z+}}$ is the selectivity coefficient for the exchange reaction, Me^{z+} is the exchangeable cation, X^- and represents a negatively charged exchange site and all quantities on the right are activities. Following the Gaines-Thomas convention (Gaines & Thomas 1953) the activities of the exchangeable cations are assumed to be equal to the equivalent fractional occupancies. The selectivity coefficients for Ca^{2+}, Mg^{2+} and Sr^{2+} were taken from Pearson et al. (2011). For the selectivity coefficient of K^+, the value derived by Gaucher et al. (2009) was used (Table 2). The exchanger composition obtained from our measurements (section 4.4) was fixed to constrain the cation concentrations in solution.

Celestite dissolution was assumed for constraining sulphate concentrations. For one model case, however, sulphate was assumed to be constrained by gypsum rather than by celestite (section 5.4). For constraining the carbonate system and pH, calcite dissolution and a fixed pCO_2 were assumed. The latter was based on pCO_2 measurements (section 4.8). The applied solubility constants are listed in Table 2. No other mineral phases, notably no silicate phases were included in the model, as detailed in section 5.4.2.

Table 1: Cation exchange and mineral dissolution reactions and their equilibrium constants at T = 25°C considered in the equilibrium model.

Reaction	**logK**	**Ref.**
Exchange reactions:		
$NaX + K+ \Leftrightarrow KX + Na^+$	1.2	1
$2NaX + Ca^{2+} \Leftrightarrow CaX_2 + 2Na^+$	0.7	2
$2NaX + Mg^{2+} \Leftrightarrow MgX_2 + 2Na^+$	0.7	2
$2NaX + Sr^{2+} \Leftrightarrow SrX_2 + 2Na^+$	0.7	2
Calcite:		
$CaCO_3 + H^+ \Leftrightarrow Ca^{2+} + HCO_3^-$	1.849	3
Celestite:		
$SrSO_4 \Leftrightarrow Sr^{2+} + SO_4^{2-}$	-6.632	3
Gypsum:		
$CaSO_4 \cdot 2H_2O \Leftrightarrow Ca^{2+} + SO_4^{2-} + 2H_2O$	-4.581	3

1: Gaucher et al. (2009); 2: Pearson et al. (2011) ; 3: Hummel et al. (2002)

An important uncertainty regards the measured Sr content on the exchanger. Celestite dissolution during the cation exchange experiments may affect this parameter, thus leading to its overprediction (Gaucher et al. 2009). The Sr-SO_4 system is therefore underconstrained in the equilibrium model. To account for this, Gaucher et al. (2009) and Mäder (2009) considered a pre-equilibration step of the exchanger with the solution assuming a fixed SO_4/Cl ratio. Here we considered two cases: in the first case, the Sr content on the exchanger was set to zero, implicitly assuming a very low Sr content on the exchanger. With this assumption, the equilibration of the cation exchanger and the reacting mineral phases with solution could be carried out in one step. In the second case, an analogous procedure to Gaucher et al. (2009) and Mäder (2009) was adopted: in a pre-equilibration step the measured exchanger composition including the measured Sr content was equilibrated with a solution containing a fixed SO_4/Cl molar ratio of 0.15. The selection of this ratio was based upon previous modelling in Opalinus Clay (Pearson et al. 2003). In a second step, the resulting solution and exchanger composition was equilibrated with the reacting mineral phases.

The geochemical code PHREEQC, version 2 (Parkhurst & Appelo 1999) and the Nagra/PSI database (Hummel et al. 2002) was used for the equilibrium modelling exercise. The objectives were (i) to test the adequacy of the model to simulate in-situ porewater chemistry data and (ii) to evaluate the overall consistency of the data. The modelling results were then compared with data from squeezing.

Because the main focus of the modelling was to evaluate the consistency of the measured data, which were all obtained at room temperature, we chose to assume 25 °C for the calculations presented in section 5.3. This is somewhat lower than the in-situ temperature of the studied sediment sequence (~45 °C, Chapter 2). As indicated from scoping calculations, the effect of this higher temperature on the solute concentrations is rather small (< 5%), except for alkalinity (or total dissolved carbonate), which is about 35% lower because of the retrograde calcite solubility.

4. Results

4.1 Mineralogical composition

XRD data

The mineralogical composition of the standard samples determined by XRD is listed in Table SI-3 (S.I.). Depicting the main mineral components (clay minerals, carbonates and quartz & feldspars) in a triangular plot (Fig. 2) after Füchtbauer (1988), illustrates the clay-rich nature of the majority of the samples. Most of the Opalinus Clay and Lias samples plot within a narrow range, representing calcareous sandy clayrocks. The 'Brown Dogger' samples show a larger variation than the underlying rock units, spreading from calcareous sandy clayrocks to sandy-argillaceous limestones. The overlying Effingen Member samples are argillaceous limestones.

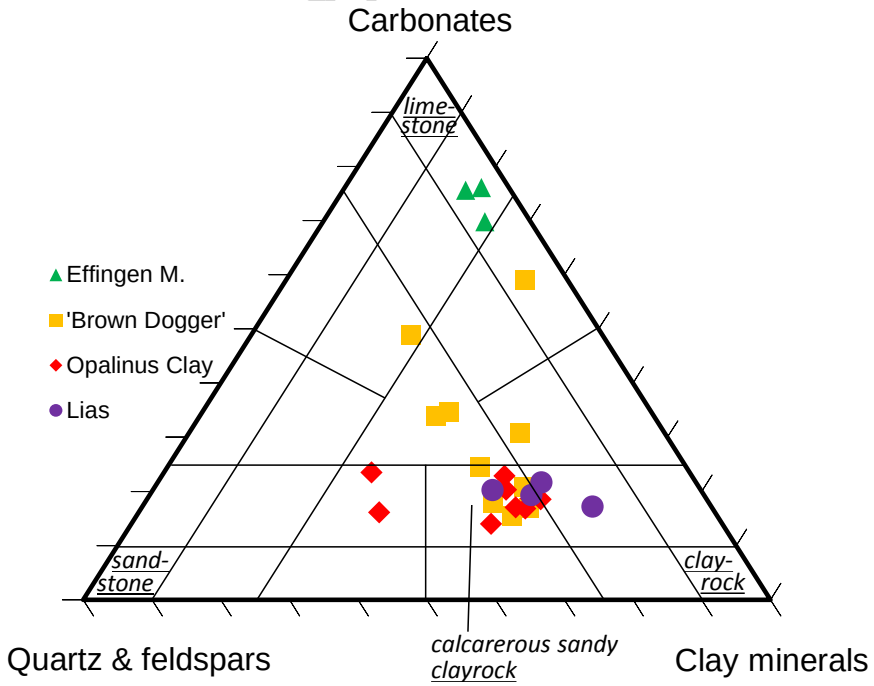

Fig. 2 Distribution of the three main mineral fractions for standard samples (classification after Füchtbauer 1988)

Clay minerals in the fraction <2 µm include mainly illite, illite/smectite (I/S) mixed layers with illite proportions of 75–85%, and kaolinite, whereas chlorite contents are mostly subordinate (Table SI-3, S.I.). The total clay-mineral content spans from 18 to 65%, displaying an increasing trend with depth in the upper section ('Brown Dogger') down to about 800 m depth, but no trend further down in the sequence (variation of 35–65%) is indicated (Fig. 3). There is a fairly large variability in the proportion of clay minerals, the largest fraction being illite (average ±1σ = 23±6 % of total clay), I/S mixed layers (49 ±8) and kaolinite (20±6) (see Table SI-3). The relative proportions of clay minerals are relatively constant and show no depth trends.

The sum of carbonate minerals is anti-correlated with the clay-mineral content (r^2 = 0.716). Thus, the carbonate contents show a decreasing trend from 18-45% in the 'Brown Dogger' to fairly constant average levels of 20% in the Opalinus Clay and Lias. The main carbonate mineral is calcite. Other carbonate minerals identified by XRD are siderite, ankerite and dolomite.

The quartz contents vary between 3–40%. In most of the profile, i.e. in the 'Brown Dogger' and Opalinus Clay units, the quartz content is fairly constant in the range of 17–27%, but two samples in the middle Opalinus Clay exhibit higher contents of 40%. The upper most unit of the Effingen Member exhibits low contents of 3–5%.

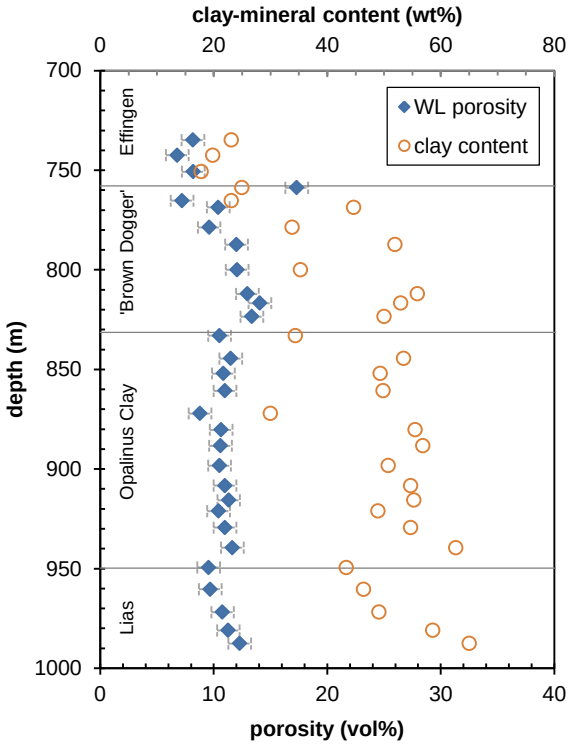

Fig. 3 Water-loss (WL) porosity and clay-mineral content vs. depth.

Diagenetic and vein minerals

The relative age sequence of diagenetic minerals was determined on the basis of microtextural features observed in thin-sections and SEM images to the degree possible. It is evident that pyrite, siderite and part of the calcite formed early, i.e. in the unconsolidated mud, while the time of precipitation for the other minerals is less clear but likely related to burial diagenesis. Pyrite is omnipresent as massive concretions, framboids and replacements of fossil calcite/aragonite structures. It was also observed in veins in the Effingen Member and the Lias. Authigenic siderite occurs as concretions and as disseminated rhombohedral crystals. Calcite is the most frequent diagenetic mineral (Fig. 4) and most abundant cementing phase occurring in larger proportions in silty and sandy parts with low fractions of clay. It is also the main mineral in veins, which are abundant in the upper part of the profile (Effingen Member and 'Brown Dogger'). Dolomite and ankerite formed as dispersed rhombohedral crystals and as cement. Chalcedony partially replacing fossil carbonate fragments was observed in one sample in the 'Brown Dogger'. Authigenic quartz was observed as tiny euhedral grains in a fine-grained diagenetic matrix between detrital quartz grains and also as growth rims of detrital quartz. Authigenic kaolinite was found in one sample of the 'Brown Dogger' and forms a fine-grained matrix between detrital quartz grains. Diagenetic Sr-Ba sulphate was observed in five out of six analysed samples (Fig. 4) where it occurs as elongated grains with lengths up to several hundreds of μm. From its interstice-filling texture it can be deduced that this sulphate phase formed late in the succession of diagenetic minerals. The elemental SEM/EDX analysis indicates the presence of Ba, varying from a few to about 60 wt%. Celestite was identified by optical microscopy in one vein in the 'Brown Dogger' (Fig. 4).

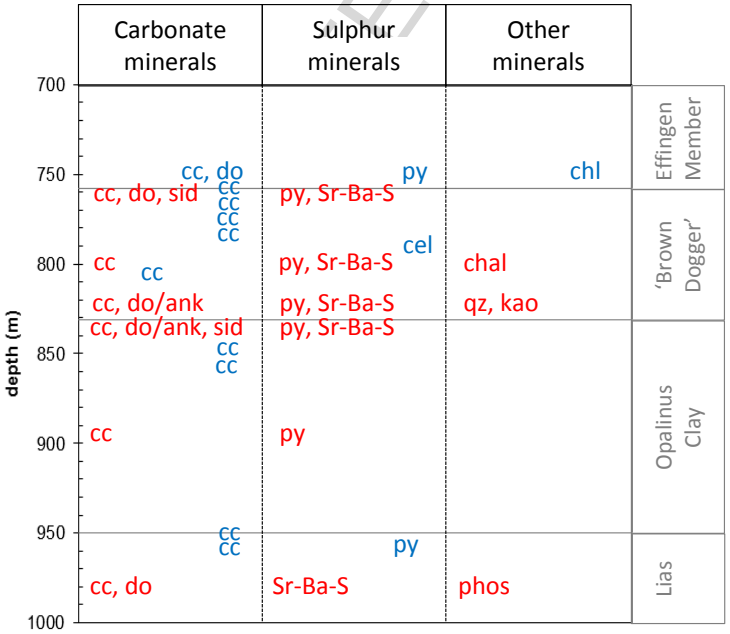

Fig. 4 Observed diagenetic minerals on 6 samples (red) and vein minerals on 10 samples (blue) from microscopic analysis as function of depth. cc: calcite; do: dolomite; ank: ankerite; sid: siderite; py: pyrite; Sr-Ba-S: Sr-Ba sulphate; cel: celestite; chl: chlorite; chal: chalcedony; kao: kaolinite; phos: phosphorite

4.2 Porosities

The data for gravimetric wet water content (hereafter termed water content), grain density and water-loss (WL) porosity are given in Table SI-4 (S.I.). An increasing trend in the WL porosity from 740 m down to a depth of 840 m is noted (Fig. 3). One sample representing an oolitic horizon enriched in iron-oxides falls off this trend and displays a higher WL porosity of 15 vol%. Below, the Opalinus Clay and Lias units exhibit WL porosities of 9–12 vol%.

The increase of porosity with depth in the upper section is related to the clay-mineral content which increases concomitantly (Figs. 3 and 5). The positive correlation with the clay-mineral content is explained by the small particle sizes for clays and large external and internal specific surfaces, to which water adsorbs.

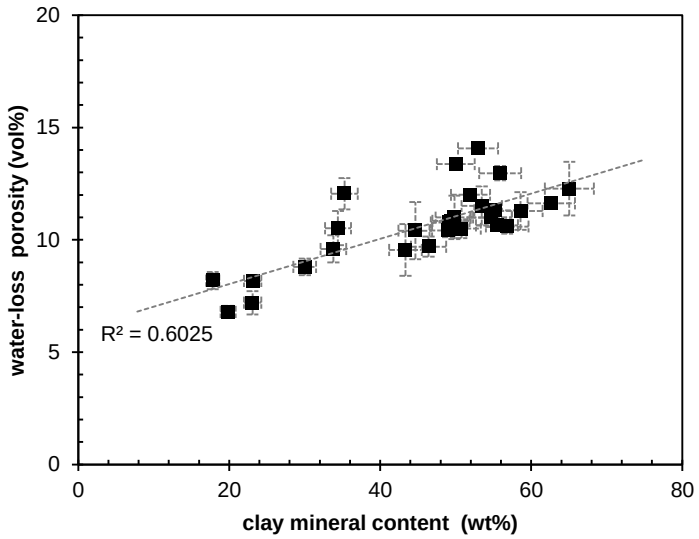

Fig. 5 Water-loss porosity as a function of the clay-mineral content

4.3 Aqueous extraction data

With the determination of the soluble compounds of argillaceous rocks in aqueous extracts, valuable information on porewater composition can be obtained (e.g. Pearson et al. 2003, Gaucher et al. 2009). However, only for non-reactive compounds occurring predominantly in the porewater, such as for chloride, can the in-situ amount in the porewater be directly back calculated. Cations are affected by cation exchange and mineral dissolution/precipitation reactions during the extraction. Trends obtained from variations in S/L ratios in the extracts combined with chemical equilibrium calculations may provide insight into such processes. In the case of cations, the concentrations of Ni-en extracted cations may further help to constrain chemical conditions in porewaters.

Table 2 shows selected averaged compositions of each of the two subsamples (series a, b) versus depths. The complete analyses for all 126 subsamples are given in Table SI-5 (S.I.). In general, the standard deviation thereof reveals fairly small values, thus indicating fairly homogeneous rock material at the scale of ~0.1 m.

Trends as function of S/L ratios

The chloride concentrations in the aqueous extracts show a linear behaviour with increasing S/L ratio for all samples (not shown) with a high correlation coefficient (r^2>0.99). When plotting concentrations per unit mass of rock, constant concentrations within analytical uncertainty are revealed, as shown for selected samples in Fig. 6a. Sodium, the main cation in the extracts, shows a different behaviour, namely a non-linear decrease with increasing S/L (Fig. 7a). This hints at cation exchange reactions which are strongly affected by the S/L ratio (Appelo & Postma, 2005). In fact, under dilute conditions divalent cations, such as Ca^{2+} and Mg^{2+}, are preferentially sorbed to the clay, leading to the displacement of Na^{+} into solution. This postulated cation exchange reaction is supported by the Na^{+} data but not by that of Ca^{2+}. Ca^{2+} concentrations do not indicate an opposite trend, but show a decrease at lower S/L ratios and fairly constant values at higher S/L ratios (Fig. 7b). A similar trend is noted for Mg^{2+} (not shown). This behaviour may be explained by the dissolution of carbonate phases such as calcite and dolomite (see section below) occurring concurrently with cation exchange reactions. These reactions are further explored by modelling calculations in section 5.3.

Sulphate concentrations depict a fairly similar linear behaviour as chloride when plotted per volume of aqueous extract (not shown). The plot of sulphate concentrations normalised per unit mass of rock, however, indicates a slight decrease in sulphate (within 15%) with S/L ratio (Fig. 6b).

Table 2 Solute concentrations of aqueous extracts, each analysis corresponds to average of 2 subsamples (see also Table SI-5, S.I.)

Sample ID	geologic unit	S/L g/g	Na mg/L	K mg/L	Ca mg/L	Mg mg/L	Sr mg/L	Cl mg/L	SO_4 mg/L	Alk meq/L	pH
SLA 734.89	Effingen M.	0.10	51.5	8.10	1.05	0.34	0.07	6.5	37.6	1.70	9.21
		0.25	96.7	11.69	1.35	0.47	0.10	16.0	92.5	2.44	9.02
		0.50	159.2	15.72	2.17	0.72	0.15	32.3	173.5	2.93	8.89
		1.00	263.5	22.72	4.29	1.51	0.31	66.6	342.3	3.32	8.64
SLA 742.48	Effingen M.	1.00	261.2	22.43	3.84	1.49	0.30	68.8	327.0	3.32	8.58
SLA 750.73	Effingen M.	0.10	47.7	8.05	1.22	0.35	0.08	6.2	34.3	1.57	9.31
		0.25	91.8	11.59	1.30	0.45	0.10	15.2	87.4	2.34	9.15
		0.50	146.3	15.94	2.17	0.72	0.15	30.7	160.1	2.93	8.98
		1.00	246.0	22.97	4.24	1.41	0.29	63.2	310.3	3.49	8.73
SLA 758.79	'Brown Dogger'	1.00	487.7	47.70	27.18	3.93	1.08	408.8	450.8	3.78	8.18
SLA 765.31	'Brown Dogger'	1.00	224.3	21.32	2.30	0.73	0.17	87.5	166.3	4.51	8.69
SLA 768.62	'Brown Dogger'	1.00	231.4	16.46	1.67	2.34	0.13	117.4	165.4	3.56	8.79
SLA 778.70	'Brown Dogger'	0.10	60.7	6.27	0.77	1.58	0.05	11.3	21.3	2.22	9.58
		0.25	94.0	9.23	0.54	0.45	0.05	29.4	50.3	3.15	9.42
		0.50	151.4	12.49	0.86	0.48	0.08	61.4	99.0	3.75	9.18
		1.00	246.2	16.81	1.73	0.49	0.15	123.6	191.0	3.39	8.59
SLA 787.33	'Brown Dogger'	1.00	272.4	17.23	3.02	0.67	0.20	159.1	236.4	2.76	8.69
SLA 800.01	'Brown Dogger'	1.00	284.6	29.41	3.15	0.72	0.23	143.4	301.4	2.91	8.67
SLA 812.11	'Brown Dogger'	0.10	64.8	6.23	0.41	0.49	0.04	14.3	16.6	2.66	9.44
		0.25	104.9	8.60	0.50	0.46	0.05	37.8	44.5	3.32	9.32
		0.50	161.4	11.11	0.75	0.26	0.07	78.0	81.5	3.92	8.89
		1.00	262.2	14.42	1.63	0.46	0.14	160.0	155.3	3.66	8.81
SLA 816.73	'Brown Dogger'	1.00	273.1	15.61	2.55	0.59	0.17	184.8	194.7	2.92	8.42
SLA 823.53	Brown Dogger'	0.10	68.5	5.81	0.41	0.32	0.03	14.8	18.2	2.55	9.44
		0.25	107.8	7.68	0.60	0.91	0.05	39.1	41.5	3.35	9.32
		0.50	162.4	10.13	0.74	0.33	0.07	82.0	82.4	3.68	8.89
		1.00	253.5	14.90	1.70	0.38	0.14	166.5	157.6	3.34	8.81
SLA 833.08	Opalinus Clay	1.00	288.7	24.66	3.92	1.14	0.27	175.1	154.5	4.99	8.55
SLA 844.56	Opalinus Clay	0.10	66.2	5.93	0.68	0.31	0.05	14.2	21.5	2.40	9.07
		0.25	118.9	8.42	0.95	0.25	0.07	36.6	52.5	3.73	8.98
		0.50	188.2	11.78	1.68	0.41	0.12	75.3	98.9	4.73	8.76
		1.00	307.8	17.48	3.78	0.96	0.24	149.8	181.8	6.07	8.57
SLA 852.06	Opalinus Clay	1.00	317.1	16.80	3.28	0.86	0.22	155.7	162.6	6.44	8.55
SLA 860.77	Opalinus Clay	0.10	70.7	5.91	0.73	0.24	0.05	15.2	24.5	2.52	9.13
		0.25	128.4	9.12	1.45	1.75	0.11	38.7	59.8	3.89	9.95
		0.50	204.6	12.49	1.93	0.48	0.15	80.2	110.3	5.07	8.70
		1.00	333.4	18.46	4.35	1.01	0.31	158.6	213.5	6.47	8.63
SLA 872.12	Opalinus Clay	1.00	311.5	18.85	4.82	1.14	0.43	154.2	210.9	5.59	8.53
SLA 880.30	Opalinus Clay	1.00	305.0	14.57	2.91	0.66	0.21	159.5	191.1	5.43	8.54
SLA 888.33	Opalinus Clay	1.00	349.7	17.42	4.44	1.13	0.33	162.6	173.6	8.02	8.48
SLA 898.31	Opalinus Clay	1.00	302.4	13.18	2.62	0.69	0.20	153.6	173.7	5.78	8.56
SLA 908.32	Opalinus Clay	1.00	351.7	16.23	4.18	1.14	0.28	145.6	191.1	8.02	8.51
SLA 915.67	Opalinus Clay	0.10	85.0	6.85	1.19	0.28	0.07	14.7	19.3	3.36	8.61
		0.25	157.1	10.07	1.98	0.48	0.12	37.4	49.3	5.56	8.63
		0.50	257.4	14.20	3.50	0.91	0.22	76.0	94.6	8.17	8.45
		1.00	407.6	19.54	6.50	1.74	0.39	151.5	172.9	10.99	8.38
SLA 921.15	Opalinus Clay	1.00	372.5	16.98	5.05	1.29	0.33	151.8	188.0	8.62	8.53
SLA 929.40	Opalinus Clay	1.00	307.8	12.81	2.79	0.64	0.19	133.3	218.0	5.62	8.90
SLA 939.48	Opalinus Clay	1.00	313.3	12.87	2.85	0.63	0.18	149.3	257.5	4.59	9.03
SLA 949.45	Opalinus Clay	0.10	36.0	5.95	2.10	0.43	0.10	7.0	24.3	1.35	9.43
		0.25	77.7	8.83	1.78	0.47	0.10	17.2	60.7	2.19	9.06
		0.50	126.1	11.66	2.32	0.61	0.13	35.1	108.9	2.99	9.12
		1.00	213.9	15.71	3.90	0.97	0.20	72.2	208.8	3.82	8.96
SLA 960.38	Lias	1.00	323.0	15.75	4.21	1.11	0.41	129.9	364.4	3.31	9.06
SLA 971.89	Lias	0.10	69.6	4.81	0.66	1.59	0.04	7.5	21.1	2.91	9.86
		0.25	110.6	6.07	0.55	1.01	0.04	19.1	56.0	3.78	9.29
		0.50	162.3	7.95	0.51	0.20	0.05	39.6	99.4	4.81	8.96
		1.00	249.3	11.26	1.22	0.57	0.09	83.4	201.7	4.54	8.78
SLA 981.04	Lias	0.10	75.5	4.38	0.43	0.92	0.02	6.7	18.8	3.06	9.28
		0.25	115.8	6.23	0.72	1.05	0.03	16.7	50.4	4.42	9.21
		0.50	166.8	7.81	0.56	0.24	0.04	34.7	93.8	5.59	9.00
		1.00	255.6	11.37	1.58	1.13	0.09	73.3	180.8	5.83	8.73
SLA 987.61	Lias	1.00	232.0	13.72	1.01	0.32	0.06	52.2	161.1	6.43	8.88

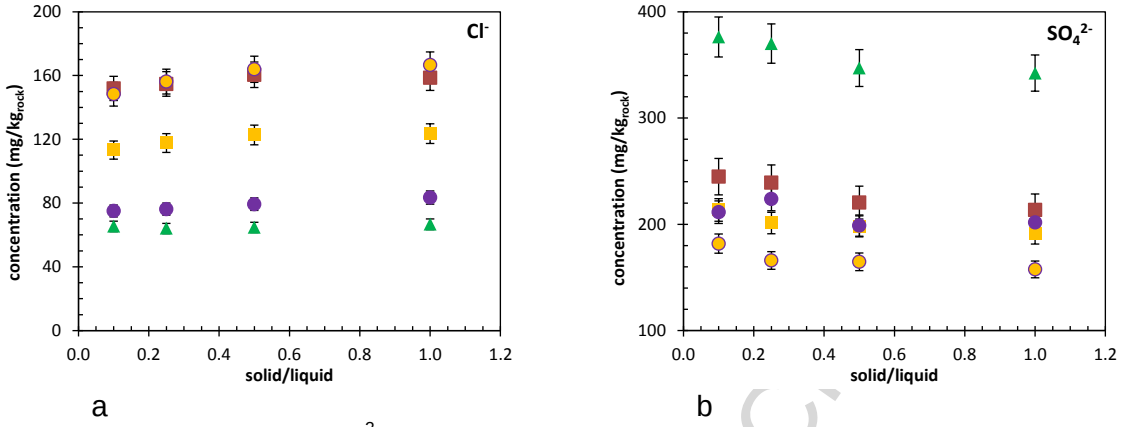

a b

Fig. 6 a) Cl^- and b) SO_4^{2-} concentration of aqueous extracts (mg/kg rock) vs. S/L ratio (g/g); symbols: green – Effingen M. (SLA 734.89), light brown – 'Brown Dogger' (square: SLA 778.70, circle: SLA 823.53), red – Opalinus Clay (SLA 860.77), purple – Lias (SLA 971.89)

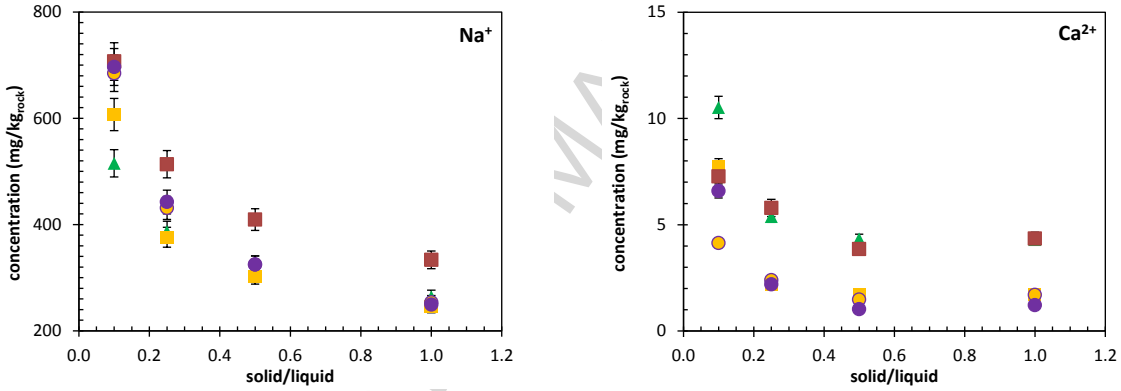

a b

Fig. 7 a) Na^+ and b) Ca^{2+} concentration (mg/kg rock); symbols: same as in Fig. 6.

Saturation indices

Speciation calculations for aqueous extracts were performed with the PHREEQC version 2 code (Parkhurst & Appelo 1999) and the Nagra/PSI database (Hummel et al. 2002). Partial pressures of CO_2(g) and saturation indices (SI) of selected potentially forming minerals are given for the aqueous extracts at S/L = 1.0 for subsamples of series a [1] in Table 3. CO_2 partial pressures (pCO_2) were calculated from alkalinity and pH measurements. The resulting values for the 1:1 aqueous extracts are within a narrow range of $\log(pCO_2) = -3.26 \pm 0.26$ bar, 1σ). All extracts are generally fairly close to saturation with respect to calcite, although there is a considerable spread in SI, ranging from -0.59 to 0.31. On the other hand, all solutions are undersaturated with regard to dolomite which is present in the majority of the samples (Fig. 4, Table SI-3, S.I.), suggesting kinetic constraints preventing dolomite equilibrium during the extraction tests. The aqueous extracts are also undersaturated with regard to gypsum or celestite. This also holds for fluorite.

[1] The calculated values for series b (not shown here) are very similar to those of series a.

Table 3 Calculated pCO_2 and saturation indices for aqueous extracts with S/L = 1 of series a

Sample ID	geol. unit	log pCO_2	SI calcite	SI dolomite(dis)	SI gypsum	SI celestite	SI strontianite	SI fluorite
SLA 734.89	Eff. M.	-3.42	-0.12	-1.00	-2.38	-1.83	-0.80	-0.93
SLA 742.48	Eff. M.	-3.42	-0.20	-1.07	-2.49	-1.87	-0.80	-1.04
SLA 750.73	Eff. M.	-3.49	-0.03	-0.82	-2.43	-1.90	-0.72	-1.32
SLA 758.79	BD	-2.85	0.20	-0.73	-1.60	-1.30	-0.73	-0.91
SLA 765.31	BD	-3.27	-0.23	-1.23	-2.92	-2.35	-0.89	-1.55
SLA 768.62	BD	-3.55	-0.33	-1.03	-3.08	-2.47	-0.95	-1.27
SLA 778.70	BD	-3.37	-0.51	-1.84	-2.98	-2.32	-1.07	-1.30
SLA 787.33	BD	-3.51	-0.23	-1.42	-2.59	-2.10	-0.96	-1.24
SLA 800.01	BD	-3.52	-0.29	-1.50	-2.59	-2.02	-0.94	-1.51
SLA 812.11	BD	-3.56	-0.27	-1.39	-3.08	-2.44	-0.86	-1.26
SLA 816.73	BD	-3.17	-0.59	-2.10	-2.73	-2.24	-1.32	-1.02
SLA 823.53	BD	-3.60	-0.30	-1.54	-3.07	-2.47	-0.93	-1.33
SLA 833.08	OPA	-3.10	-0.01	-0.88	-2.70	-2.18	-0.72	-1.39
SLA 844.56	OPA	-3.13	0.09	-0.68	-2.68	-2.18	-0.63	-1.58
SLA 852.06	OPA	-3.01	-0.03	-0.93	-2.81	-2.27	-0.72	-1.69
SLA 860.77	OPA	-3.11	0.14	-0.63	-2.60	-2.03	-0.51	-1.71
SLA 872.12	OPA	-3.07	0.06	-0.79	-2.54	-1.88	-0.51	-1.73
SLA 880.30	OPA	-3.10	-0.15	-1.22	-2.79	-2.22	-0.80	-1.71
SLA 888.33	OPA	-2.87	0.12	-0.64	-2.68	-2.11	-0.53	-1.80
SLA 898.31	OPA	-3.07	-0.15	-1.13	-2.86	-2.28	-0.79	-1.92
SLA 908.32	OPA	-2.91	0.13	-0.59	-2.66	-2.13	-0.56	-1.86
SLA 915.67	OPA	-2.63	0.31	-0.23	-2.54	-2.05	-0.43	-1.86
SLA 921.15	OPA	-2.87	0.29	-0.29	-2.55	-2.03	-0.42	-1.80
SLA 929.40	OPA	-3.38	0.08	-0.76	-2.77	-2.23	-0.60	-1.62
SLA 939.48	OPA	-3.69	0.17	-0.60	-2.71	-2.19	-0.54	-1.68
SLA 949.45	OPA	-3.63	0.19	-0.52	-2.58	-2.17	-0.62	-1.70
SLA 960.38	Lias	-3.89	0.19	-0.47	-2.42	-1.71	-0.33	-1.09
SLA 971.89	Lias	-3.34	-0.41	-1.32	-3.08	-2.54	-1.10	-1.24
SLA 981.04	Lias	-3.24	-0.12	-0.56	-2.96	-2.50	-0.89	-1.11
SLA 987.61	Lias	-3.35	-0.19	-1.18	-3.25	-2.81	-0.97	-1.38

4.4 CEC and exchangeable cation data

Normalised per mass of rock, the Ni consumption, which is thought to approximate the cation exchange capacity (CEC), should be equal for the different S/L ratios used, if side reactions, such as mineral dissolution, do not significantly affect the CEC (Bradbury & Baeyens 1997/1998).

Table 4 depicts the CEC data (as Ni consumption) and the concentrations of the main cations for the six samples extracted with Ni-en at S/L ratios of 0.1−1.0. The CEC shows some variation with S/L ratio (up to 50%) with no consistent trend between the samples.

Table 4 Data of Ni-en extract solutions for selected standard samples

Sample ID	S/L	Geologic unit	Na	K	Mg	Ca	Sr	Sum Cations	Ni consumpt.
			meq/kg	meq/kg	meq/kg	meq/kg	meq/kg	meq/kg	meq/kg
SLA 742.48	0.10	Effingen M.	31.40	11.82	19.80	58.78	0.93	122.7	83.0
SLA 742.48	0.25		31.48	13.95	15.44	30.58	0.72	92.2	93.9
SLA 742.48	0.50		30.98	8.49	12.69	22.77	0.64	75.6	90.3
SLA 742.48	1.00		28.56	7.75	11.58	20.56	0.58	69.0	76.0
SLA 787.33	0.10	'Brown Dogger'	54.58	13.83	16.61	74.17	1.17	160.4	122.4
SLA 787.33	0.25		55.34	12.70	14.16	42.64	1.19	126.0	173.9
SLA 787.33	0.50		49.43	11.14	13.28	35.94	1.08	110.9	129.0
SLA 787.33	0.99		49.62	8.18	11.88	28.64	1.00	99.3	117.0
SLA 816.73	0.10	'Brown Dogger'	64.27	17.28	16.64	50.16	1.37	149.7	201.6
SLA 816.73	0.25		62.26	9.92	15.47	51.66	1.29	140.6	170.5
SLA 816.73	0.50		58.81	7.42	13.23	40.54	1.29	121.3	151.7
SLA 816.73	1.00		60.42	9.48	11.81	33.71	1.20	116.6	132.6
SLA 860.77	0.10	Opalinus Clay	50.32	10.82	14.13	70.51	1.19	147.0	108.8
SLA 860.77	0.25		50.33	9.92	12.11	29.36	1.14	102.9	141.1
SLA 860.77	0.50		46.40	8.29	11.02	19.29	1.05	86.0	120.8
SLA 860.77	1.00		47.37	7.57	10.75	15.92	0.94	82.5	101.4
SLA 898.31	0.11	Opalinus Clay	56.92	10.52	14.68	43.20	1.18	126.5	119.7
SLA 898.31	0.25		55.47	9.82	14.36	36.30	1.15	117.1	157.9
SLA 898.31	0.50		51.38	7.85	11.60	32.47	1.07	104.4	125.1
SLA 898.31	0.99		52.81	6.92	11.32	18.55	1.00	90.6	110.7
SLA 971.89	0.10	Lias	58.36	10.95	14.96	55.18	0.81	140.3	147.6
SLA 971.89	0.25		56.33	9.86	12.08	36.71	0.75	115.7	142.9
SLA 971.89	0.51		52.28	8.28	10.85	24.62	0.72	96.7	120.3
SLA 971.89	1.00		54.96	7.02	10.15	20.42	0.68	93.2	111.8

The concentrations of exchangeable cations reveal more conspicuous differences with S/L compared to CEC data. This is illustrated in Fig. 8. Sodium shows relatively constant values (differences are within 10%) at all S/L ratios. The exchangeable divalent cations show a much more marked increase with decreasing S/L ratio. This is attributed to the enhanced dissolution of carbonates and perhaps also of sulphate minerals (*cf.* section 5) at lower S/L ratios because of stronger complexation of the divalent cations with ethylenediamine (section 3.2). Potassium also exhibits a marked increase in the Ni-extracts at lower S/L ratios; the reason is unclear. Similar trends for Ca, Mg and K were observed in previous Opalinus Clay studies (Pearson et al. 2003, Appendix A3), but the effect was much smaller there, because the Ni-en concentration had been adjusted to the S/L ratio whereas they were set to be the same concentration for all S/L ratios in this work (cf. Methods section).

Overall, the behaviour of cations in the Ni-extracts indicates that these are less affected by side reactions at high S/L compared to low S/L ratios. The sum of cations at S/L=1 shows fair agreement with the CEC values derived from Ni consumption (differences are 9–19%), but the latter data are systematically higher. The possible reasons are discussed in section 5.3.

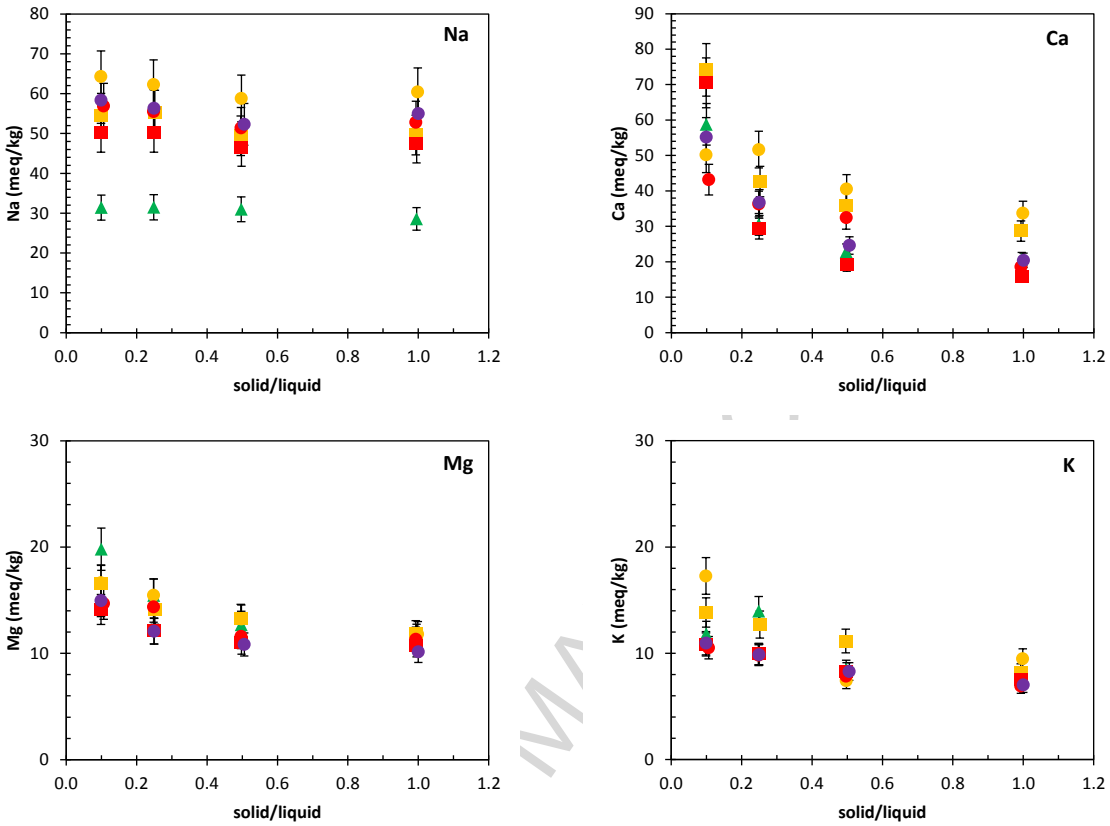

Fig. 8 Cation concentrations (meq/kg$_{rock}$) in Ni-extract vs. S/L ratio

The trend of CEC with depth follows that of the clay-mineral content (Fig. 9). This trend is expected as the CEC is predominantly induced by the structural negative charge of the smectite and illite minerals. With the known amounts of these minerals, the theoretical CEC can be estimated. This has been done based on the illite, smectite, kaolinite and chlorite fractions determined by XRD (Table SI-3, S.I.) and the CEC data for these clay minerals. For illite a CEC value of 225 meq/kg (Baeyens & Bradbury 2004) was assumed. The CEC for smectite (869 meq/kg) was assumed to correspond to that of MX-80 montmorillonite (Karnland et al. 2006). Both kaolinite and chlorite have small but measurable CEC, assumed to be 30 meq/kg for kaolinite and 50 mg/kg for chlorite (Allard et al. 1983). The resulting CEC data depicted in Fig. 9 reveals the good agreement of these calculated data with the CEC data measured by Ni consumption. Thus, the difference is within 6% except for the sample from the Effingen Member with the lowest CEC where the difference is 31%. This general agreement is quite remarkable in view of the considerable uncertainties related to the estimated CEC data from mineralogy. On the other hand, the difference, although fairly small, between Ni consumption and sum of cations (see above) points to some methodological uncertainty related to the Ni extraction data. The CEC and population of exchangeable cations are discussed in section 5.3.

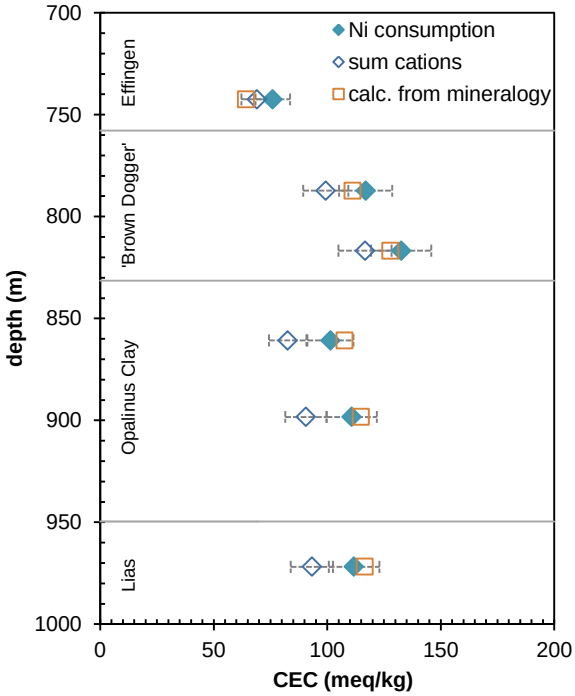

Fig. 9 Ni consumption as proxy for the cation exchange capacity (CEC), sum of cations in the Ni-en extract solutions and calculated CEC from illite, smectite contents (meq/kg_{rock}) versus depth for S/L = 1

4.5 Squeezing data

As indicated in section 3.2.5, porewaters were obtained from squeezed samples at squeezing pressures of 200–500 MPa. Moreover, aqueous extracts from the core material after squeezing were obtained. The resulting data and their interpretation in the light of the effect of squeezing on porewater chemistry have recently been reported (Mazurek et al. 2015). From this analysis, it was found that increasing squeezing pressures affect the major ions. Thus, with increasing squeezing pressure, Cl^- and Na^+ are presumably affected by ion filtration, whereas Ca^{2+} and Mg^{2+} are affected by pressure-driven carbonate mineral dissolution. As an important conclusion, the analysed porewater chemistry at the lowest squeezing pressure (i.e. 200 MPa) was found to be the least affected by the above mentioned effects. Because this work focusses on the in-situ porewater chemistry, we limit ourselves here to the presentation of the lowest squeezing pressure data as well as the aqueous extracts from the samples after squeezing.

Table 5 shows the chemical analyses of waters squeezed at the lowest pressure of 200 MPa. The composition for all waters is dominated by Na and Cl. Sulphate and Ca are the second most important anion and cation, respectively. Note that, because of the very small sample volumes and methodological constraints, no measurements of alkalinity and pH were conducted for the squeezed waters presented here. Therefore the saturation states with regard to carbonate minerals cannot be calculated. The waters are slightly undersaturated with respect to gypsum (SI = -0.7 to -0.2) and closer to saturation with respect to celestite (SI -0.4 to -0.1) (see discussion in section 5.2).

Table 5 Chemical composition, petrophysical parameters, clay-mineral content and total chloride concentration of waters squeezed at 200 MPa

Sample ID	**geol. unit**	**Na**	**K**	**Ca**	**Mg**	**Sr**	**Cl**	**Br**	**SO_4**	**SI gypsum** [b]	**SI celestite**[b]	**water content** [c]	**grain density**	**Water-loss porosity** [d]	**Total Cl** [e]	**clay content**
		mg/L	mg/L	mg/L	mg/L	mg/L	mg/L	mg/L	mg/L	-	-	wt%	g/cm^3	vol%	mg/kg$_{rock}$	wt%
SLA 780.66	BD	3321.4	75.0	423.3	106.3	15.5	5133.6	6.1	1283.4	-0.53	-0.21	4.60	2.726	11.62	121.84	49
SLA 796.53		3350.6	79.7	487.2	111.7	19.0	5319.6	6.1	1390.3	-0.45	-0.12	5.59	2.805	14.24	167.96	47
SLA 807.51		4605.9	108.8	482.1	99.4	17.4	6966.5	8.0	1273.5	-0.54	-0.26	3.62	2.775	9.44	127.87	28
SLA 816.93		3525.0	76.6	497.9	111.4	17.4	5685.8	6.2	1210.1	-0.50	-0.23	4.84	2.729	12.20	152.26	47
SLA 825.65		3389.7	77.1	535.1	125.8	21.7	5482.6	6.0	1298.8	-0.45	-0.10	5.03	2.779	12.84	151.34	39
SLA 878.45	OPA	4061.8	80.5	514.3	105.4	17.1	6351.3	6.5	1323.8	-0.49	-0.23	3.84	2.795	10.05	132.19	45
SLA 896.31		4568.9	100.6	528.4	108.0	17.2	7356.3	7.1	981.6	-0.62	-0.37	3.86	2.798	10.11	138.86	54
SLA 915.87		3563.7	77.1	553.5	127.7	18.5	5820.5	5.6	1162.9	-0.49	-0.22	4.20	2.782	10.88	139.10	56
SLA 937.89		3620.4	61.6	579.8	132.3	18.6	5725.9	5.9	1572.9	-0.36	-0.11	5.01	2.740	12.62	147.35	71
SLA 958.21[a]	Lias	4221.4	83.1	519.8	113.0	15.9	6058.4	6.0	2178.4	-0.30	-0.08	3.74	2.565	9.06	107.05	45
SLA 987.40		2340.5	47.2	164.5	34.4	<10	2408.0	2.6	1929.6	-0.66	-0.15	4.87	2.679	12.05	48.75	63

[a] squeezed at 300 MPa
[b] calculated assuming a pH of 7.5 for all samples
[c] calculated from sum of squeezed waters and gravimetric water content of remaining core
[d] calculated from water content (squeezed water + water obtained from water loss of squeezed core) and grain density
[e] calculated from sum of chloride mass in squeezed waters and mass in extracts of core (all squeezing pressure steps)

Bromide shows a similar behaviour as chloride in squeezed samples. The Cl/Br mass ratios are in the range of about 800−1000, thus considerably above that of seawater (~290), and indicate a slightly increasing trend with depth in the 'Brown Dogger' and upper part of the Opalinus Clay.

4.6 Groundwater sample from the 'Brown Dogger'

A groundwater sample was taken from the 'Brown Dogger' during hydraulic testing (hydrotest "BD1") in the depth interval 799.25–833.50 m. The composition of the sample and that of the drilling fluid (traced with uranine) is presented in Table SI-6 (S.I.). As indicated from the high DOC and the presence of uranine and tritium, the groundwater sample shows contamination by the drilling fluid. From the DOC and uranine concentrations, the fraction of the drilling fluid in the groundwater sample is 33%, from tritium a higher fraction of 51% is derived. The fraction of the Cl, SO_4, Br and Na in the groundwater is roughly estimated by assuming contamination in the range of 33–51%. The resulting concentration of these compounds is 5459−5520 mg/L for Cl, 1209−1270 mg/L for SO_4, 4−5 mg/L for Br and 3643−2760 mg/L for Na.

4.7 CO_2 partial pressure data

As described in section 3.2.7, gas/core equilibrium was considered to be attained when the amounts of CO_2 and alkanes and corresponding gas partial pressures tended to reach a steady state. As depicted in Fig. 10, this state was reached for the majority of samples at about 90−100 days. One sample (SLA 976.55, not shown) clearly showed no trend of reaching a plateau after more than 300 days and was not considered for pCO_2 estimation. For three samples (i.e. SLA 858.14, SLA 889.08, SLA 974.50), the last point shows an increase above the "plateau" values (Fig. 10); these last points were in fact affected by an increase in O_2/N_2 ratio and therefore not taken into account for the estimation of pCO_2. For sample SLA 947.28, there is a lack of points between 35 days and the last two points at 178/195 days. Because of the similar values as compared to the adjacent Opalinus Clay samples, it was assumed that steady-state conditions were reached at 178/195 days.

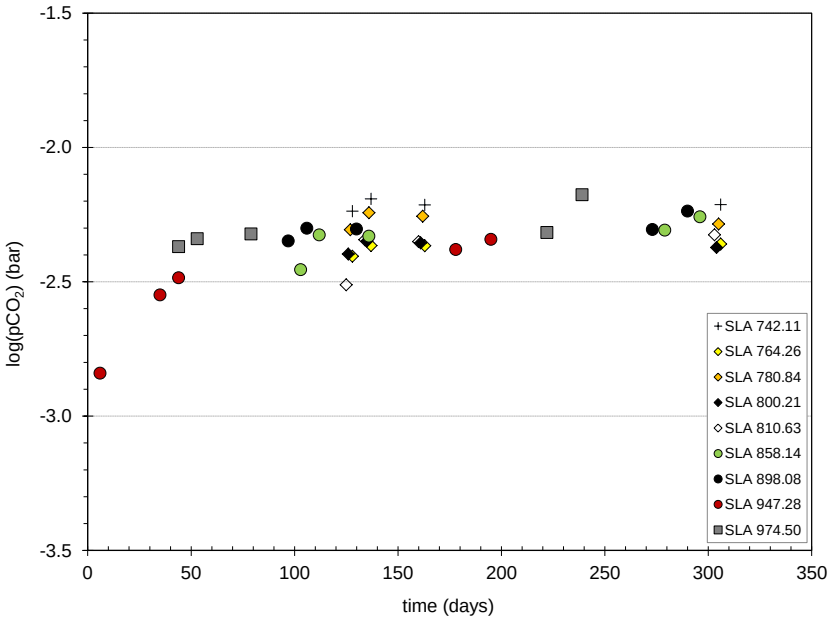

Fig. 10: Evolution of the CO_2 partial pressure in the ten gas cells during the solid/gas equilibration time.

From these considerations and otherwise assuming that the last point reflects equilibrium pCO_2 in the core, the pCO_2 values were derived (Table 6). These values are fairly constant ($10^{-2.5}$–$10^{-2.2}$ bar) throughout the analysed rock profile (Fig. 10). It is interesting to note that this range is similar to that obtained from earlier pCO_2 measurements in Opalinus Clay samples from the Mont Terri URL (Lassin et al. 2003, Lerouge et al. 2015). Table 6 also depicts the contents and partial pressures of alkanes (CH_4, C_2H_6 and C_3H_8).

Table 6 Measurements of the partial pressures of CO_2, CH_4, C_2H_6, C_3H_8 in the gas assuming that solid/gas equilibrium is attained. Analytical uncertainties of gas measurements are 3% and those of total pressure are 3 mbar.

sample ID	**time** day	**P_{total}** Mbar	**pCO_2** log(bar)	**pCH_4** log(bar)	**pC_2H_6** log(bar)	**pC_3H_8** log(bar)
SLA 742.11	308	662	-2.21	-3.45	-4.14	-4.28
SLA 764.26	306	685	-2.36	-3.25	-3.94	-4.19
SLA 780.84	305	682	-2.29	-2.72	-3.51	-3.79
SLA 800.10	304	667	-2.37	-2.94	-3.81	-4.04
SLA 810.63	303	690	-2.33	-3.00	-3.87	-4.05
SLA 854.14	279	667	-2.31	-2.57	-3.41	-3.40
SLA 898.08	273	635	-2.31	-2.35	-3.24	-3.13
SLA 947.28	195	615	-2.34	-3.48	-4.08	-3.80
SLA 974.50	222	1031	-2.32	-2.48	-3.33	-3.22

The CO_2/(CO_2+alkanes) ratios were constant at later times (not shown) for the gas cells where no leak occurred. The gas is a mixture of CO_2 and alkanes, with CO_2/(CO_2+alkanes) ratios ranging between 0.44 in the Opalinus Clay Formation (sample 898.08 m) to 0.92 in rocks of the Effingen Member (sample 742.11 m). A further observation was the general decrease of the C1/(C2+C3) ratios with time, whereas the C2/C3 ratios remained stable. The decrease of the C1/(C2+C3) ratios with time could be related to differences of rates of gas diffusion due to the different molecule sizes.

In the gas cells which were opened for stopping a leak (SLA 947.28, SLA 976.55) or having a leak without gas cell opening (SLA 974.50), the CO_2/(CO_2+alkanes) ratios showed irregular behaviour and a sharp rise after gas cells had been opened (not shown). Moreover, C1/(C2+C3) ratios were much lower than in the other gas cells. The observations indicate that alkanes were depleted in reconditioned gas cells while for CO_2 this was not the case. This result corroborates previous work of Lassin et al. (2000), strongly suggesting a control of the partial pressure by the initial stock of dissolved gas for alkanes but not for CO_2. CO_2 is regenerated by the porewater via re-equilibration with the carbonate system and the buffer capacity of the mineralogical assemblage. This result is in agreement with previous results repeatedly shown on clayrock, such as Opalinus Clay or the Callovo-Oxfordian Formation (COx) and gives confidence in the pCO_2 measurements shown here. It further suggests that the measured final pCO_2 can be used as a proxy for in-situ CO_2 partial pressure, even though it is difficult to evaluate the true in-situ pCO_2 values (Lassin et al. 2012).

5. Discussion

5.1 Chloride concentrations and anion-accessible porosity

The depth profile for chloride from squeezing data (red squares) is shown in Fig. 11. Chloride shows no trend in most of the profile, displaying a concentration range of about

5000–7000 mg/L. In the lowest part of the Lias, a distinctly lower concentration of about 2000 mg/L is revealed. The trend towards lower salinity with depth is due to the likely presence of low-salinity water in the underlying Keuper aquifer. In the nearby Benken borehole, a similar depth trend of chloride was identified and was explained by Gimmi & Waber 2007 and Mazurek et al. 2011) as a diffusion profile that evolved since the flushing of the Keuper aquifer with fresh water was initiated (see Section 2). The same trend is found for the aqueous extraction data re-calculated for water-loss porosity (Fig. 11a, open blue circles). However, these data consistently show lower concentrations compared to the squeezing data. This is attributed to anion exclusion induced by the structural negative charge in the smectite and illite fraction and a deficit of anions relative to cations in the electric double layers at the clay surfaces (Tournassat & Appelo 2011). This ion exclusion effect is commonly approximated by the concept of anion-accessible porosity or "geochemical" porosity (Pearson 1999; Pearson et al. 2003), although in reality the decrease of anions towards the negatively charged surface represents a continuum rather than a step function.

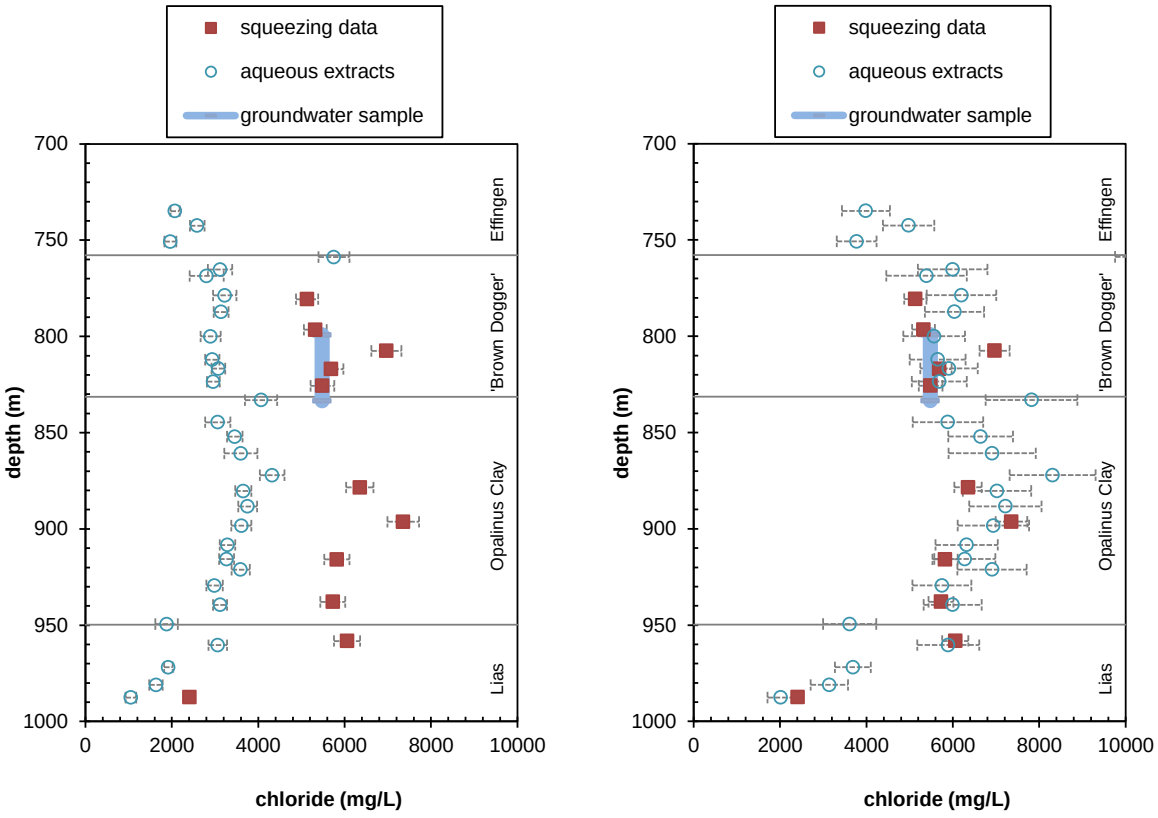

Fig. 11 Chloride concentrations in squeezed waters, calculated from aqueous extracts (S/L=1), and in a groundwater sample as function of depth; a) concentration in aqueous extracts back-calculated to water-loss porosity; b) concentration in aquoeus extracts back-calculated to a constant anion-accessible porosity fraction of 0.52.

As outlined in section 1, an anion-accessible porosity of about 50% of the water-filled porosity (porosity fraction of 0.5) has been proposed for Opalinus Clay (Pearson et al. 2003; Gimmi & Waber 2004, Appelo & Wersin 2007, Mazurek et al 2011, Gimmi et al. 2014). Using

this anion-accessible porosity fraction, Mazurek et al. (2015) could show that the Cl^- concentrations in the porewater obtained by aqueous extraction showed good correspondence with the measured concentrations of squeezed waters at 200 MPa. Here we adopt the reverse approach and derive the anion-accessible porosity fraction from the chloride concentrations in the squeezed waters. The results are then compared with other data from aqueous extraction and sampled groundwater for plausibility. Assuming that the chloride concentrations $C_{Cl\text{-}\_sq}$ (mg/L) in the squeezed waters (at 200 MPa) represent the in-situ porewater concentrations, the anion-accessible porosity fraction (α) can be derived from:

$$\alpha = \frac{m_{Cl}}{w_w \cdot C_{Cl^-\_sq}} \quad (3)$$

where m_{Cl} is the Cl^- inventory (mg/kg wet rock) and w_w is the wet water content as (L/kg wet rock). The corresponding data are listed in Table 5. The derived anion-accessible porosity fraction values are in the range of 0.42−0.56, with an average value of 0.52 ($\pm$ 0.05 1σ). It does not depict any trend with clay-mineral content over the whole range of 28−65% (Fig. 12). A positive correlation might be expected, because the amount of negatively charged minerals increases with the clay-mineral content. As outlined in section 1, a similar anion-accessible porosity fraction of around 0.5 has been derived for different argillaceous units with variable clay-mineral content in Europe (Mazurek et al. 2011), such as the Callovo-Oxfordian (Gaucher et al. 2009) or the Effingen Member (Mazurek et al. 2012). The reason for the observed constant anion-accessible porosity fraction over a large range of clay-mineral content has, to the best of our knowledge, not yet been resolved. A possible explanation is that the major part of porosity is associated with the clay fraction distributed in a (nearly) nonporous carbonate-tectosilicate material. Support for this explanation is provided by the observed positive correlation of porosity with clay-mineral content (Fig. 5).

Ionic strength is a further parameter which affects the thickness of the electric double layers and the anion-accessible porosity. The total chloride concentrations (as proxy for ionic strength) in aqueous extracts and squeezed waters are fairly constant, but decrease markedly in the lowest part in the Lias unit (Fig. 11). The sample from the lowest part (SLA 987.40) displays a distinctly lower anion-accessible porosity fraction (0.42) compared to the other samples (Fig. 12). This could be related to the lower ionic strength and the concomitant thicker electrical double layers.

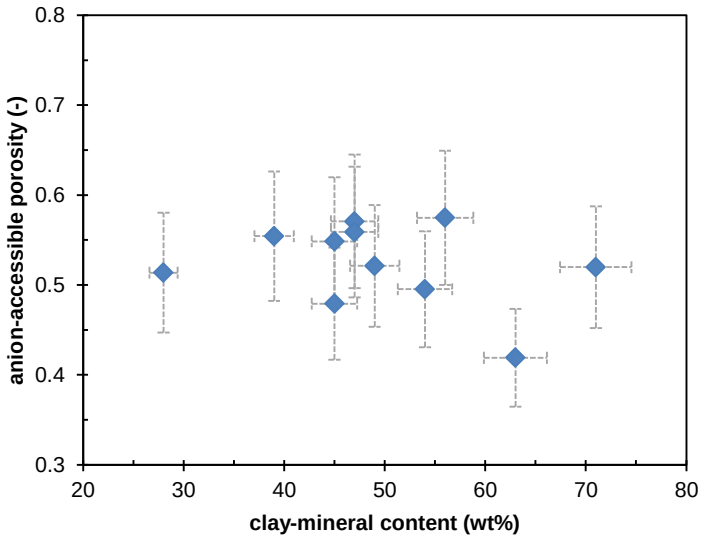

Fig. 12: Anion-accessible porosity fraction derived from chloride data of squeezed samples as function of clay-mineral content (Table 4). Error of anion-accessible porosity was estimated to be 13% based on linear error propagation of analytical errors.

The anion-accessible porosity was also evaluated by using chloride data from sample pairs of squeezed waters and back-calculated aqueous extracts (1:1), the latter selected from closest location of the squeezed sample. Again, anion-accessible fractions according to eq. (2) were calculated. The resulting values (not shown) are very similar to those obtained from squeezing data alone, with an average value of 0.55 ($\pm$ 0.06 1σ). This is also apparent from the similar chloride depth profile of the back-calculated aqueous extraction and squeezing data (Fig. 11b). Hence, the total Cl contents of the aqueous extracts is consistent with the total Cl contents of the squeezing data. Further support is provided by the results from the groundwater sample in the 'Brown Dogger'. The Cl concentration in the groundwater is near-identical to that obtained from three squeezed samples located in the same section, which supports the assumption that squeezing data closely represent in-situ porewater compositions. A fourth squeezing sample in the same interval yields a somewhat higher value.

5.2 Constraining sulphate concentrations in the porewater

Sulphate concentrations obtained from different methods as a function of depth are shown in Fig. 13. The data for squeezed waters show good agreement with that from the groundwater sample suggesting that these reflect in-situ porewater conditions. The profile is fairly constant with depth, but exhibits an increasing trend in the lower part of the rock sequence. This may reflect the influence of sulphate-rich water from the lower lying aquifers (Waber et al. 2014).

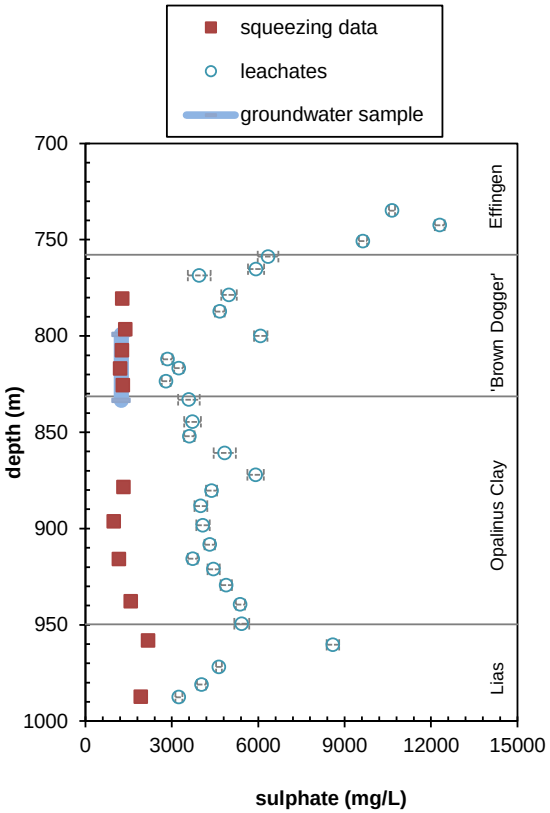

Fig. 13 Sulphate concentrations in squeezed waters, aqueous extracts (back-calculated to water-loss porosity) and the groundwater sample from the 'Brown Dogger' vs depth

The aqueous extracts, back-calculated to water-loss porosity show a different trend and much higher sulphate concentrations compared with the other data (Fig. 13). Considering anion exclusion, the apparent discrepancy becomes even larger. This "excess sulphate" indicated from the extracts points to a sulphur source releasing sulphate during extraction into the porewater. Potential sources are pyrite, sulphur bound in organic matter and sulphate mineral phases. The calculated "excess sulphate" is in the range of 1-3 mmol per kg rock corresponding to a very low proportion (< 2 %) of the total sulphur in the rock.

Pyrite oxidation during the extraction tests is considered to be insignificant. In fact, precautions were taken to minimise the contact with molecular O_2 by conducting sample preparation and extraction tests in an anaerobic glovebox (section 3.2.3). The most likely possibility of aerobic oxidation was during milling which was carried out outside the glovebox. Pyrite oxidation rates in air are generally in the range of 10^{-7}–10^{-8} mol $O_2/m^2/s$ (Jerz 2002). Assuming spherical pyrite grains of 1µm (estimated from SEM images), the surface area can be estimated from geometric considerations (Nicholson 1994), which yields a value of 1.2 m^2/g. From the pyrite content (Table SI-3, S.I.), assuming a high oxidation rate of 10^{-7} O_2 mol/m^2/s, and a milling time of 10 min., one obtains 0.07–1.6 mmol SO_4 per kg rock. This is about 5–70% of the "excess sulphate", thus too low to fully explain aqueous extraction data, but could represent a significant contribution. Preliminary unpublished tests in our laboratory have been conducted to evaluate the effect of sample preparation on sulphate concentration in the aqueous extracts. These suggest that the effect of pyrite

oxidation is small, lending more support to a lower oxidation rate than assumed in the above calculation.

Release of sulphur from organic matter as sulphate source is considered to be unlikely because from mass balance this would require that the organic matter would contain 10–20% of sulphur. Moreover, all this “organic” sulphur would need to have been oxidised during the experimental procedure of the aqueous extraction tests.

Dissolution of sulphate minerals, such as celestite or gypsum, is a viable possibility to explain “excess sulphate” observed in aqueous extraction data. From a mass balance, the "excess sulphate" would correspond only to 0.14–0.41 g $CaSO_4$ or 0.18–0.55 g $SrSO_4$ per kg of rock. Such minor phases – assuming this is the total amount – would not be detected by XRD.

Diagenetically-formed Sr-Ba sulphate was observed by SEM/EDX in five out six samples at different locations and celestite (with unknown composition) was identified in one vein sample from ‘Brown Dogger’ by optical microscopy (Fig. 4). Diagenetic Sr-Ba sulphate and celestite-infill in a tectonic fracture were recently identified in Opalinus Clay at the Benken site (Lerouge et al. 2014). Gypsum or anhydrite were not observed in this work. Diagenetic gypsum was reported from an Opalinus Clay sample from the Mont Terri site (Bläsi et al. 1990). Other evidence for authigenic gypsum or anhydrite in Opalinus Clay is lacking so far. Squeezing data are not entirely in line with a gypsum (or anhydrite) source, because they show slight undersaturation with $CaSO_4$ phases in squeezed waters (SI values -0.2 to -0.5) (Table 5). Squeezed waters are slightly closer to saturation with regard to celestite (SI -0.1 to -0.4). Celestite has been proposed to control sulphate porewater in the Callovo-Oxfordian shale (Gaucher et al. 2009).

Based upon the above considerations, sulphate in the analysed porewaters seems most likely controlled by celestite equilibrium or a $SrSO_4$-containing solid solution phase. Further work is required to support this conclusion, in particular to determine the mineral chemistry of sulphate-bearing phases in these argillaceous rocks.

5.3 Constraining cation exchange population

The results obtained from the different methods indicate that the concentration of cations in the porewater is controlled by cation exchange and mineral reactions, such as carbonate and sulphate equilbria. The impact of cation exchange is illustrated in the non-linear behaviour of main cations as function of S/L ratios in the aqueous extracts (section 4.3). Here we analyse cation exchange in the extracts in more detail and derive the exchangeable cation population at different S/L ratio from the dissolved ions by applying a cation exchange model with aid of the speciation code PHREEQC (Parkhurst & Appelo 1999) and selectivity coefficients proposed in Pearson et al. (2011). Model details and results are provided in the Supporting Information, Table SI-7.

Fig. 14 shows the ratio of exchangable Ca and Na (CaX_2/NaX) calculated for the aqueous extracts at the lowest S/L (0.1) and highest S/L (1.0) ratios, respectively. A clear decrease of this ratio with increasing S/L is evident, which is explained by the preferential uptake of Ca^{2+} relative to Na^+ at higher dilution. Note also that at higher dilution of the extracts the scatter in the calculated exchange cation population is larger, reflecting the effect of enhanced mineral dissolution. The same trends are exhibited by the other exchangable divalent cations Mg^{2+}

and Sr^{2+} (not shown). The CaX_2/NaX ratios determined from Ni-ethylene displacement (section 4.4) are also depicted in Fig. 14. These are fairly close to those obtained from the high S/L extracts, albeit somewhat lower in some cases.

In summary, the cation composition in the porewater cannot be directly obtained from aqueous extraction data because of concurrent cation exchange reactions and mineral dissolution reactions, particularly at low S/L ratios. It appears from equilibrium considerations, however, that the exchanger population at high S/L ratio is fairly close to the in-situ ones.

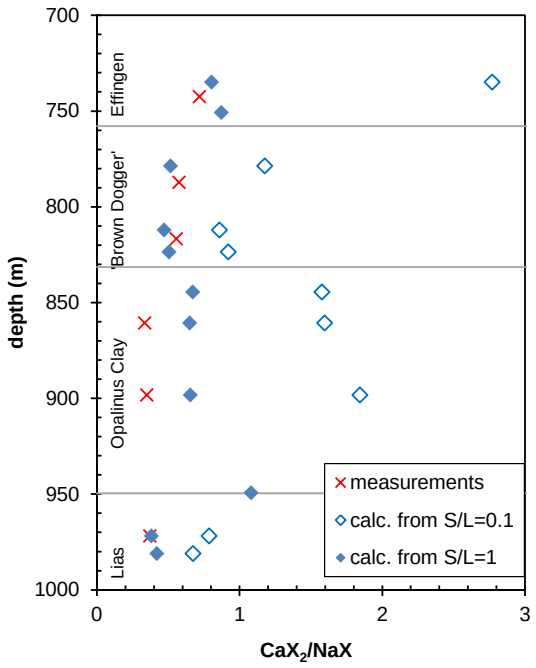

Fig. 14 Ratio of exchangable Ca and Na as equivalent fractions as function of depth. Data of aqueous extracts (S/L = 0.1 and S/L = 1.0) calculated with cation exchange model. Measured data from Ni extracts (S/L =1) shown as comparison.

As outlined in section 4.4, the CEC data derived from Ni consumption in the 1:1 extracts show good agreement with the CEC values estimated from the smectite and illite contents. The CEC derived from the sum of displaced cations by the Ni-en complex is somewhat lower. The reason for this difference is not clear and in fact an opposite result could be expected, because measured Ni-displaced cations should represent both exchangeable and dissolved fractions. The same observation, however, was made in previous studies (Bradbury & Baeyens 1998, Pearson et al. 2003). Possible reasons for higher CEC obtained from Ni consumption compared to the sum of cations are: (i) formation of polynuclear Ni surface complexes and/or Ni (co)precipitates and (ii) sorption of Ni^{2+} to amphoteric oxide-type surface sites (Bradbury & Baeyens 1998). It should be noted that in contrast to the exchange population the uncertainty in the absolute CEC values are not relevant for equilibrium modelling presented below.

5.4 Equilibrium modelling of porewater compositions

5.4.1 Selection of samples / input data

The modelling procedures are presented in section 3.3. Rock sections were considered for which aqueous extraction, CEC/exchangeable cation data and squeezing data were available. This resulted in five sections, two from the 'Brown Dogger', two from Opalinus Clay and one from the Lias unit (Table SI-9, S.I.). The input data for the modelling are based on the findings and discussions in the previous sections, as summarized here:

Chloride: The Cl pore water concentrations were derived from the aqueous extraction concentration (for data at S/L=1) by accounting for the water content and an anion-accessible porosity of 0.5.

Sulphate: Celestite and/or Sr-Ba sulphate are considered as the most likely contributors for porewater sulphate, but the presence of gypsum is also evaluated here. In all calculated cases, SO_4 is assumed to be controlled by equilibrium with sulphate minerals with the same anion-accessible porosity fraction as for chloride. As detailed in section 3.3, Sr is underconstrained because of the uncertainty related to exchangeable Sr data. This uncertainty also affects that of sulphate concentrations when celestite equilibrium is assumed (Gaucher et al. 2009, Mäder 2009). To account for this, we consider two cases: in the first, the initial exchangeable Sr content is set to zero. In the second case, which is similar to that proposed by Gaucher et al. (2009), the measured exchangeable Sr content and a fixed SO_4/Cl molar ratio of 0.15 is used as input.

Exchangeable cations and selectivity coefficients: The cationic compounds Na, Ca, Mg, K and Sr are constrained by cation exchange reactions occurring at the clay surface and mineral equilibrium. The in-situ population of the exchangeable cations - a part from Sr (see above) - is taken here from the measured Ni-ethylene extraction data at the highest S/L ratio (1:1). Of particular importance are the ratios of the exchangeable cations. However, these are uncertain because of the poorly constrained contributions of the dissolved cations on one hand and of mineral dissolution on the other. In view of this, two bounding cases with regard to Na/Ca and Na/Mg ratios are considered: (i) use of measured data without further corrections, (ii) correction of measured data by assuming that Na compensates the charges of Cl and SO_4 in the aqueous extracts. Thus in case (ii) the measured Cl and SO_4 are attributed to Na and this case reflects "low" Na/Ca and Na/Mg ratios, whereas case (i) reflects "high" Na/Ca and Na/Mg ratios.

Mineral equilibria: Equilibrium with calcite, omnipresent in the rock sequence, is accounted for. For constraining sulphate, two cases, namely equilibrium with celestite and gypsum are considered. Preliminary SEM-EDX analysis (section 4.1) indicates the occurrence of a Sr-Ba-SO_4 phase rather than pure celestite. Hence, the lower solubility of such a phase may lead to a slight overestimation of SO_4 if equilibrium with pure celestite is assumed. Dolomite is present as accessory mineral in most of the samples, but indications for Opalinus Clay at Mont Terri (Pearson et al. 2011) and the Callovo-Oxfordian shale at Bure (Gaucher et al. 2009) suggest that porewaters are slightly undersaturated. These authors proposed to constrain Mg concentrations by cation exchange rather than by dolomite equilibrium. This assumption is also adopted here. Siderite is present as accessory mineral in more than half of analysed samples. Together with pyrite this phase has been used to constrain dissolved Fe concentrations in Pearson et al. (2003; 2011). Furthermore, Fe(II) control by Na^+-Fe^{2+}

exchange has been considered (Gaucher et al. 2009; Pearson et al. 2011). In this work, neither dissolved Fe or exchangeable Fe(II) were analysed and therefore Fe equilibria are not included in the modelling. Silicate phases, such as clay minerals and quartz, present in abundant amounts in the rock sequence, are expected to control Si and Al in the solute and have been postulated to also control pH/pCO_2 conditions (Coudrain-Ribstein & Gouze 1993; Gaucher et al. 2009). The main obstacle in considering silicates in equilibrium calculations is the lack of information regarding stability constants of the actual silicate minerals in the rock formations, except for quartz and kaolinite. Being aware of this deficiency, Pearson et al. (2011) assumed different pairs of generic silicate minerals. In this work, Si and Al concentrations were not determined. Because these concentrations are low and only marginally influence those of the major compounds, they were not included in the present modelling.

pH/pCO_2 conditions: Generally speaking, there have been two proposed ways two to constrain to pH/pCO_2 conditions in clayrocks, i.e. (i) by fixing pCO_2 (e.g. Pearson et al. 2003; Mäder 2009) or (ii) equilibrium with a selected set of silicate phases (Coudrain-Ribstein & Gouze 1993, Gaucher et al. 2009). In addition, Beaucaire et al. (2000) derived the pH from fixing total carbonate and charge balancing. Here we chose to fix pCO_2, but accounting for the related uncertainty by considering a reasonable range. The pCO_2 measurements presented in section 4.7 yield direct values and are regarded as a proxy for in-situ pCO_2.The corresponding values were found to be fairly constant, with log(pCO_2) of -2.2 to -2.5 log(bar). These values are within the range of those obtained with the same technique on cores from Opalinus Clay at the Mont Terri site (-3.07 to -2.12) and from the Callovo-Oxfordian at the Bure site (-3.01 to -2.00) as reported by Gaucher et al. (2010). Based upon these data, we selected an upper value of -2.2 log(bar) as a base case and a lower one of -3.1 log(bar) as a separate case.

5.4.2 Setup of model cases

The ranges in parameters and the uncertainties were considered by different model cases. Thus, one base case (case A) reflecting the most likely conditions from our understanding, and four alternative cases (cases B to E) were set up. All cases assume calcite equilibrium. Cases A to D assume celestite and case E assumes gypsum equilibrium. In all cases except case B, the initial exchangeable Sr occupancy is set to zero and the solution is equilibrated with the exchanger and reacting mineral phases in one step. For case B, a pre-equilibration step with the exchanger is conducted before equilibrating the resulting exchanger and solution compositions with the reacting minerals (section 3.3).

Case A: The base case only considers the measured Cl concentration, re-calculated to the anion-accessible porosity fraction of 0.5, and the measured CEC and uncorrected exchangeable cation data. Celestite equilibrium is assumed. The partial pressure of CO_2 is fixed to $10^{-2.2}$ bar.

Case B: The difference with respect to the base case is that the SO_4 concentration corresponding to a SO_4/Cl molar ratio of 0.15 and the measured exchangeable Sr occupancy are added as input (see sections 3.3 and 5.4.1).

Case C: In this case the fractions of exchangeable cations measured from Ni consumption are corrected by attributing part of the measured Na to NaCl and Na_2SO_4 dissolution (Bradbury & Baeyens 1998). This correction is performed by taking the measured Cl and

SO_4 data from the aqueous extracts. This results in increased equivalent fractions of Ca, Mg, K and Sr relative to Na on the exchanger.

Case D: In this case the effect of a lower pCO_2, taken to be $10^{-3.1}$ bar, is explored.

Case E: Gypsum rather than celestite equilibrium is assumed.

Table 7 *Conditions selected for the different model cases (see text)*

	Case A ***base case***	**Case B** ***SO_4/Cl***	**Case C** ***corr. exch.cat.***	**Case D** ***low pCO_2***	**Case E** ***$CaSO_4$ eq.***
celestite or gypsum	celestite eq.	s	s	s	gypsum eq.
calcite	calcite eq.	s	s	s	s
Cl input	re-calc. extraction conc.	s	s	s	s
SO_4 input	none	SO_4/Cl = 0.15	s	s	s
Ca input	none	s	s	s	s
Na input	charge balance	s	s	s	s
pCO_2 (bar)	$10^{-2.2}$	s	s	$10^{-3.1}$	s
CEC input	Ni consumption	s	s	s	s
exchangeable cations (except Sr)	uncorr. data (Ni extracts)	s	corrected for $NaCl/Na_2SO_4$	s	s
exchangeable Sr	set to zero	measured data	s	s	s

s: same as case A

5.4.3 Results and discussion of modelling

The results for all model cases and their comparison with squeezing data are shown in Table SI-9 (S.I.) and illustrated in Fig. 15. First the model cases A through D, all assuming celestite equilibrium, are considered. Here, a good to fair agreement between experimental data from squeezing and modelling data is indicated, but systematic differences between model cases are seen. For Cl, the good match between model and data is a consequence of the observed near to constant anion-accessible porosity implemented in the model. For Na, the correspondence is within 18%. Deviations are largest for SO_4 and Sr, reflecting the uncertainty related to the sulphate source. Cases A, C and D show deviations in SO_4 relative to the squeezing data by 8–63% and are thus well within a factor of 2, but display higher values compared to the measured data. For case B, which considers the measured exchangeable Sr as input, the differences in sulphate concentrations relative to the measurements are 21–44%). For Sr, deviations are larger and range between 131 and 202%. Note that for this case the simulated Sr concentrations are consistently higher, but those of sulphate consistently lower than the measured squeezing data. This confirms that exchangeable Sr measured in the Ni-exctracts were affected by side reactions (section 3.3).

The model case E with gypsum equilibrium reveals comparatively large differences between modelled and experimental data (Table SI-9, S.I.). The largest deviations are noted for sulphate and calcium, confirming the undersaturated state of the porewater with regard to gypsum or anhydrite. Significant differences are also seen in Mg and Sr. Based on these model results, celestite equilibrium more likely controls sulphate in porewaters. It should be noted, however, that the data suggest slight undersaturation with respect to celestite. This

could be due to the presence of a Sr-Ba sulphate solid solution with a lower solubility than that of pure celestite. In view of the lack of Ba data in the sampled porewaters, we did not attempt to test this hypothesis.

The good performance of the base case A in simulating squeezed water data is remarkable. Thus, the agreement for the major compounds Na, Ca, Mg, K, Cl and SO_4 is within 30% for almost all data points, as illustrated in the Schoeller diagrams in Fig. 15. Except for SO_4, the largest deviation is found for Mg (40%) in the Opalinus Clay sample at 880 m depth. The generally good agreement supports the underlying model assumptions and also confirms the adequacy of using chloride aqueous extraction data with an anion-accessible fraction of 0.5, as well as exchangeable cation data (determined with the Ni-en method) for estimating in-situ porewater composition.

Case D (low pCO_2 case) shows nearly identical results compared to the base case for all modelled compounds except for alkalinity and pH. This highlights that the main cations are only weakly affected by pH/pCO_2 conditions and controlled predominately by cation exchange, which provides an effective buffering process. The derived pH for the low pCO_2 case is in the range of 7.6-8.0 whereas the pH values span from 7.2 to 7.5 in the other cases. The model results also illustrate that with the lack of reliable pH and alkalinity in the squeezing data the pCO_2 cannot be better constrained. Without such data (pH, alkalinity), it can also not be decided whether the squeezing data (thought to represent in-situ water) are undersaturated or in equilibrium with dolomite.

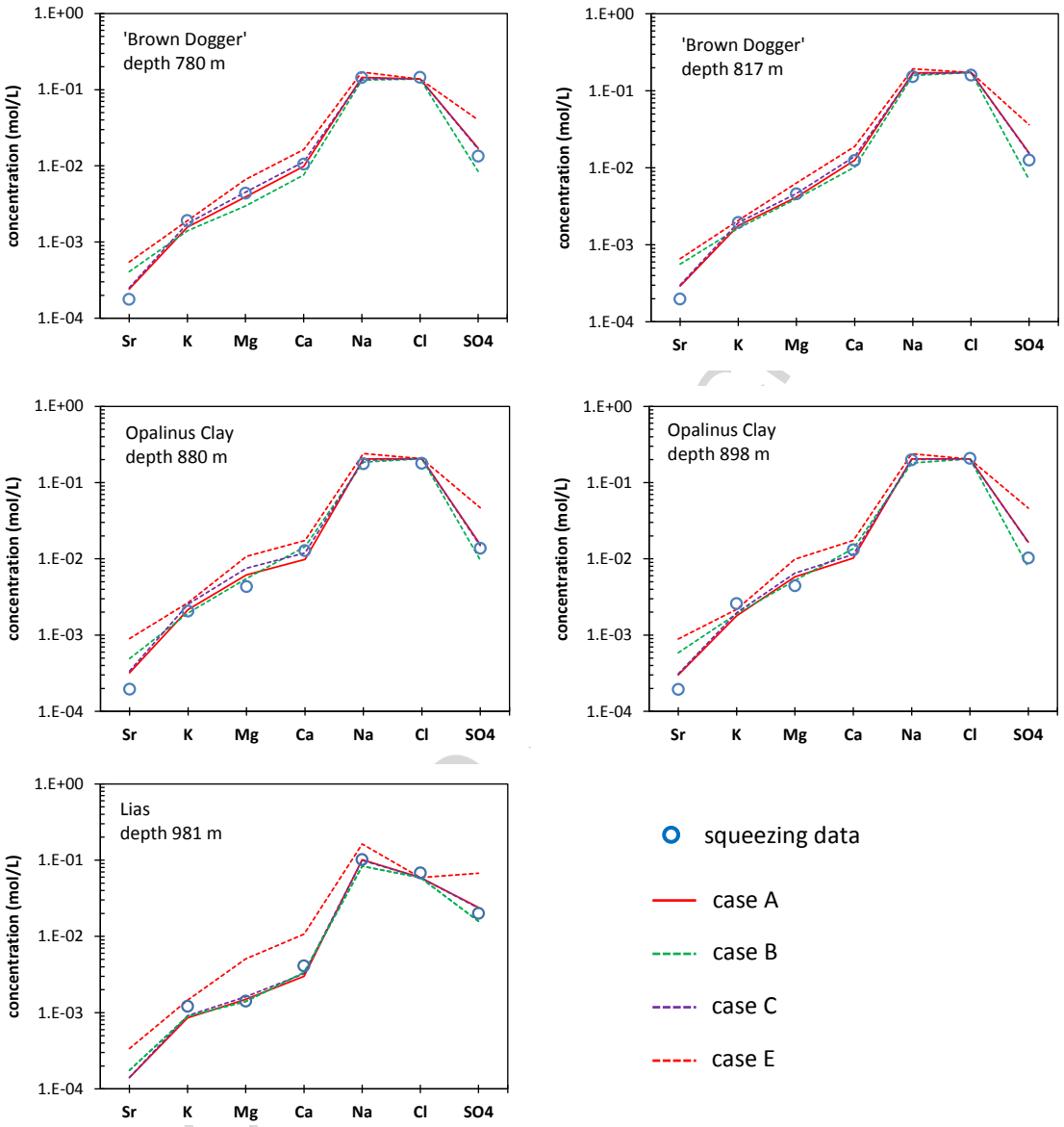

Fig. 15: Schoeller diagram comparing ion compositions from squeezing (circles) with modelled data (lines). Red solid line: case A (base case); green dashed line: case B (constant initial SO_4/Cl=0.15); case C (corrected cation exchange composition); case E (assuming gypsum equilibrium). Case D shows almost identical results to case A (see text).

The correction of exchangeable cation data by subtracting NaCl and Na_2SO_4 (case C) and thus increasing the fractions of Ca and Mg leads to less good agreement compared to cases with non-corrected fractions. This suggests that measured fractions are close to the in-situ ones and not strongly altered by side-reactions. Clearly, the dissolved cations in the porewater contribute to the Ni-displaced cations, but is seems that this “dissolved” fraction does not significantly affect exchangeable cation ratios. In this regard it should be noted that correction by subtracting NaCl and $CaSO_4$ (instead of NaCl and Na_2SO_4) results in similar exchangeable fractions than the uncorrected ones (data not shown).

In summary, the modelling exercise shows the adequacy of the simple equilibrium model and an anion-accessible porosity fraction of 0.5 in simulating porewater composition in a rock sequence with variable clay-mineral contents. It also highlights the importance of

determining the chloride inventories from aqueous extraction tests and exchangeable cation inventories from Ni-en extracts.

6. Conclusions

A multi-method approach was applied to constrain porewater chemistry in a Jurassic argillaceous rock sequence with variable lithology and clay-mineral content. In general, findings corroborate previous results from similar rocks but have also enabled uncertainties to be reduced with regard to processes affecting in-situ porewater composition. Specifically, the following findings are worth noting:

- A consistent dataset could be obtained from the different methods enabling porewater compositions to be constrained over the whole rock sequence.
- Exclusion of anions: This process is evidenced by the different chloride datasets. An anion-accessible porosity fraction of ~0.5 is derived from squeezing data for a fairly large range of clay-mineral content. A very similar result is obtained when combining squeezing data with aqueous extraction data from nearby samples. The derived anion-accessible porosity is supported by the chloride concentrations estimated from the groundwater sample.
- Source of sulphate in porewater: Consistent sulphate porewater results were obtained from squeezing and groundwater data. Sulphate is constrained by a sulphate mineral which most likely is celestite and/or a Sr-Ba sulphate phase, as indicated from microscopic analysis. Squeezed waters were found to be fairly close to saturation with regard to celestite, but undersaturated with regard to gypsum.
- Consistency of equilibrium model: The application of a simple geochemical model including cation exchange and calcite and celestite equilibria and a constant anion-accessible porosity of 0.5 showed good agreement between simulated porewater compositions and those from squeezing data. The modelling further indicated the importance of the correct determination of the exchangeable cation population, which was shown to be a sensitive parameter. More generally, the modelling analysis corroborates that squeezing of the studied rocks at 200 MPa is a viable and efficient way to sample porewater.

An important remaining uncertainty regards in-situ pH conditions. The results from CO_2 gas measurements suggest fairly constant pCO_2 conditions with $\log(pCO_2)$ values of -2.5 to -2.2 log(bar) throughout the core, but may not reflect true equilibrium conditions (Lassin et al. 2012). A $\log(pCO_2)$ range of -3.1 to -2.2 was proposed by Pearson et al. (2011) for Opalinus Clay porewaters based on calculations considering clay mineral equilibria and associated uncertainties. Our modelling results suggest that this pCO_2 uncertainty range is also reasonable for the studied rock sequence.

The concentrations of iron and, more generally, of redox conditions were not analysed in this study. Besides iron, the concentrations of other redox sensitive species in the porewater, such as sulphide are not known. The preservation of redox conditions is difficult and all applied methods may induce disturbances. The consistency in sulphate data, however, indicates that pyrite oxidation was largely suppressed during the experimental procedures.

From the widespread occurrence of siderite in the studied rock sequence, this phase may control Fe(II) concentrations. However, other Fe-bearing carbonates, such as diagenetic calcite and, at instances also ankerite are present which might influence iron equilibrium relationships. The study of the mineral chemistry of these carbonate phase assemblages may shed more light on this issue.

In addition to carbonates, the systematic study of the mineral chemistry of sulphate phases (e.g. celestite, Sr-Ba sulphates) and their distribution would allow further constraint of the sulphate concentration in porewaters.

Acknowledgements

We would like to express our thanks to Antoine de Haller, Annette Bretscher, Michael Adler, Peter Alt-Epping, Nick Waber and Larryn Diamond (Uni Bern) and Andreas Gautschi (Nagra) for fruitful discussions. Laboratory support of Priska Bähler, Stefan Weissen and Gisela Weibel (Uni Bern) is acknowledged. Squeezing tests were carried out by Takahiro Oyama and Kenzo Kiho (Criepi). The study was financially supported by Nagra.

Allard B., Karlsson M., Tullborg, E.-L. and Larson S.A. (1983) *Ion exchange capacities and surface areas of some major components and fracture filling materials of igneous rocks.* SKB Technical Report TR 83-64, Stockholm, Sweden (Available at www.skb.se).

Appelo C.A.J. and Postma D. (2005) *Geochemistry, groundwater and pollution*. Balkema, Rotterdam, 2nd edition, 649 p.

Appelo C.A.J. and Wersin P. (2007) Multicomponent diffusion modeling in clay systems with application to the diffusion of tritium, iodide and sodium in Opalinus Clay. *Environ. Sci. Technol.* **41**, 5002–5007.

Appelo C.A.J., Vinsot A., Mettler S. and Wechner S. (2008) Obtaining the porewater composition of a clay rock by modeling the in- and out-diffusion of anions and cations from an in-situ experiment. *J. Contam. Hydrol*. **101**, 67–76.

Baeyens B. and Bradbury M.H. (2004) Cation exchange capacity measurements on illite using the sodium and cesium isotope dilution technique: Effects of the index cation, electrolyte concentration and competition: modeling. *Clays Clay Miner*. **52**, 421–431

Beaucaire C., Pitsch H., Toulhoat P., Motellier S. and Louvat D. (2000) Regional fluid characterisation and modelling of water-rock equilibria in the Boom clay formation and in the Rupelian aquifer at Mol, Belgium. *Appl. Geochem*. **15**, 667–686.

Beaucaire C., Michelot J.-L., Savoye S. and Cabrera J. (2008) Groundwater characterisation and modelling of water–rock interaction in an argillaceous formation (Tournemire, France). *Appl. Geochem*. **23**, 2182–2197.

Blanc P., Legendre O. and Gaucher E.C. (2006) Estimate of clay minerals amounts from XRD pattern modeling: The ARQUANT model. *Phys. Chem. Earth* **32**, 135–144.

Bläsi H.R., Peters T. and Mazurek M. (1990) *Der Opalinuston des Mont Terri (Kanton Jura): Lithologie, Mineralogie und phys.-chemische Parameter*. Nagra Internal Report NIB 90-60, Wettingen, Switzerland.

Bradbury, M.H. and Baeyens, B. (1997/98) *Derivation of In-situ Opalinus Clay Porewater Compositions from Experimental and Geochemical Modelling Studies with Corrigendum*.

Nagra Technical Report NTB 97-07, Nagra, Wettingen, Switzerland (Available at www.nagra.ch).

Bradbury M.H., Baeyens B. (1998) A physicochemical characterisation and geochemical modelling approach for determining porewater chemistries in argillaceous rocks. *Geochim. Cosmochim. Acta* **62**, 783–795.

Coudrain-Ribstein A. and Gouze P. (1993) Quantitative study of geochemical processes in the Dogger aquifer, Paris Basin. *Appl. Geochem*. **8**, 495–506.

De Craen M., Wemaere I., Labat S. and Van Geet M. (2006) *Geochemical analyses of Boom Clay pore water and underlying aquifers in the Essen-1 borehole*. SCK.CEN External Report CEN-ER-19 (Available at http://publications.sckcen.be).

Füchtbauer H. (1988) *Sedimente und Sedimentgesteine. Schweizerbart Verlagsbuchhandlung*, Stuttgart, 1141 p.

Gaines G.L. Jr., Thomas H.C. (1953): Adsorption studies on clay minerals. II. A formulation of the thermodynamics of exchange adsorption. J. Chem. Phys. **21**, 714–718.

Gaucher E.C., Blanc P., Bardot F., Braibant G., Buschaert S., Crouzet C., Gautier A., Girard J.-P., Jacquot E., Lassin A., Negrel G., Tournassat C., Vinsot A. and Altmann S. (2006) Modelling the porewater chemistry of the Callovian-Oxfordian formation at a regional scale. Comptes Rendus. *Géoscience* **338**, 917–930.

Gaucher E.C., Tournassat C., Pearson F.J., Blanc P., Crouzet C., Lerouge C. and Altmann S. (2009) A robust model for pore-water chemistry of clayrock. *Geochim. Cosmochim. Acta* **73**, 6470–6487.

Gaucher E.C., Lassin A., Lerouge C., Fléhoc C., Marty N. C., Henry B., Tournassat C., Altmann S., Vinsot A., Buschaert S. et al. (2010) CO_2 partial pressure in clayrocks: a general model (2010). *In Water-Rock Interaction XIII* - Water-Rock Interaction WRI-13, Mexico [hal-00664967 - version 1].

Gimmi T. and Waber H.N. (2004) *Modelling of tracer profiles in pore water of argillaceous rock in the Benken borehole: stable water isotopes, chloride and chlorine isotopes*. Nagra Technical Report 04-05, Wettingen, Switzerland (Available at www.nagra.ch).

Gimmi T., Waber H.N., Gautschi A. and Rübel A. (2007) Stable water isotopes in pore water of Jurassic argillaceous rocks as tracers for solute transport over large spatial and temporal scales. *Water Resour. Res*. **43**, W04410.

Gimmi T., Leupin O., Eikenberg J., Glaus M.A., Van Loon L.R., Waber H.R., Wersin P., Wang H.A.O., Grolimund D., Borca C.N., Dewonck S. and Wittebroodt C. (2014) Anisotropic diffusion at the field scale – I: A four-year multi-tracer diffusion and retention experiment at the Mont Terri URL (Switzerland). *Geochim. Cosmochim*. Acta **125**, 373–393.

Girard J.-P., Fléhoc C. and Gaucher E. (2005) Stable isotope composition of CO_2 outgassed from cores of argillites: a simple method to constrain $\delta^{18}O$ of porewater and $\delta^{13}C$ of dissolved carbon in mudrocks. *Appl. Geochem*. **20**, 713–725.

Hummel W., Berner U., Curti E., Pearson J.F. and Thoenen T. (2002) *Nagra /PSI Thermochemical Data Base 01/01*. Nagra Technical Report NTB 02-16, Wettingen, Switzerland.

Jerz J.K. (2002) *Geochemical Reactions in Unsaturated Mine Wastes*. PhD thesis, Virginia Polytechnic Institute and State University, Blacksburg USA.

Karnland O., Olsson S. and Nilsson U. (2006) *Mineralogy and sealing properties of various bentonites and smectite-rich clay materials*. SKB Technical Report TR-06-30, Stockholm, Sweden (Available at www.skb.se).

Lassin A., Gaucher E. and Crouzet C. (2000) *Measurements of partial pressure of CO_2 and alkanes in a core of Opalinus Clay*. Mont Terri Project, Technical Note TN 200-45, Mont Terri Project, Switzerland.

Lassin A., Gaucher E.C. and Crouzet C. (2003) *Dissolved carbon dioxide and hydrocarbon extraction*. Annex 6 in: Pearson F.J. et al., Geochemistry of water in the Opalinus Clay Formation at the Mont Terri Rock Laboratory. Geology Series. No.5. Swiss Federal Office for Water and Geology. Bern, Switzerland (Available at www.swisstopo.admin.ch).

Lassin A., Marty N., Henry B., Trémosa J., Gailhanou H., Gaucher E.C., Madé B. and Altmann S. (2012) Equilibrium partial pressure of CO_2 in the Callovian-Oxfordian argillite as a function of relative humidity. *Proc. Earth Planet. Sci*. **7**, 459–462.

Lerouge C., Grangeon S., Gaucher E.C., Tournassat C., Agrinier P., Guerrot C., Widory D., Fléhoc C., Wille G., Ramboz C., Vinsot A., Buschaert S. (2011) Mineralogical and isotopic record of biotic and abiotic diagenesis of the Callovian–Oxfordian clayey formation of Bure (France). Geochim. Cosmochim. Acta **75**, 2633–2663.

Lerouge C., Grangeon S., Claret F., Gaucher E.C., Blanc P., Guerrot C., Flehoc C., Wille G. and Mazurek M. (2014) Mineralogical and isotopic record of diagenesis from the Opalinus Clay formation at Benken, Switzerland: implications for the modeling of pore-water chemistry in a clay formation. *Clays Clay Miner*. **62**, 286–312.

Lerouge C., Blessing M., Flehoc C., Gaucher E.C., Henry B., Lassin A., Marty N., Matray J.M., Proust E., Rufer D., Tremosa J. and Vinsot A. (2015) Dissolved CO_2 and alkane gas in clay formations. *Proc. Earth Planet. Sci*. **13**, 88–91.

Mäder U.K. (2009) *Reference pore water for the Opalinus Clay and "Brown Dogger" for the provisional safety-analysis in the framework of the sectorial plan - interim results (SGT-ZE).* Nagra Arbeitsbericht NAB 09-14, Wettingen, Switzerland (Available at www.nagra.ch).

Mazurek M., Hurford A.J. and Leu, W. (2006) Unravelling the multi-stage burial history of the Swiss Molasse Basin: Integration of apatite fission track, vitrinite reflectance and biomarker isomerisation analysis. *Basin Res.* **18**, 27–50.

Mazurek M., Alt-Epping P., Bath A., Gimmi T., Waber N., Buschaert S., De Cannière P., De Craen M., Gautschi A., Savoye S., Vinsot A., Wemaere and Wouters L. (2011) Natural tracer profiles across argillaceous formations. *Appl. Geochem*. **26**, 1035–1064.

Mazurek M.,Waber H.N., Mäder U.K., Gimmi T., De Haller A. and Koroleva M. (2012) *Geochemical Synthesis for the Effingen Member in Boreholes at Oftringen, Gösgen and Küttigen.* Nagra Technical Report NTB 12-07, Wettingen, Switzerland (Available at www.nagra.ch).

Mazurek M., Oyama T., Wersin P. and Alt-Epping P. (2015) Pore-water squeezing from indurated shales. *Chem. Geol*. **400**, 106–121.

Nagra (2002) *Projekt Opalinuston: Synthese der geowissenschaftlichen Untersuchungsergebnisse*. Nagra Technical Report NTB 02-03, Wettingen, Switzerland (Available at www.nagra.ch).

Nagra (2014) *SGT Etappe 2: Vorschlag weiter zu untersuchender geologischer Standortgebiete mit zugehörigen Standortarealen für die Oberflächenanlage. Geologische Grundlagen*. Nagra Technical Report NTB 14-02, Wettingen, Switzerland (Available at www.nagra.ch).

Nicholson R.V. (1994) Iron-sulfide oxidation mechanism: laboratory studies. In: J.L. Jambor & D.W. Blowes (eds.), Short Course Handbook on Environmental Geochemistry of Sulfide Mine-Waters; *Mineralogical Association of Canada* **22**, 163–184.

Parkhurst D.L. and Appelo C.A.J. (1999): *User's guide to PHREEQC (Version 2) - A computer program for speciation, batch reaction, one-dimensional transport, and inverse geochemical calculations.* U.S. Geological Survey Water-Resources Investigations Report 99-4259.

Pearson F.J. (1999) What is the porosity of a mudrock? *In: Muds and Mudstones: Physical and fluid flow properties*. Aplin A.C., Fleet A.J., Macquaker J.H.S. (eds.). Geological Society, London, Special Publications. **158**, 9-21.

Pearson F.J., Arcos D., Bath A., Boisson J.Y., Fernández A.M., Gäbler H.-E., Gaucher E., Gautschi A., Griffault L., Hernán P. and Waber H.N. (2003) *Geochemistry of water in the Opalinus Clay formation at the Mont Terri Rock Laboratory.* Geology Series. No.5. Swiss Federal Office for Water and Geology. Bern, Switzerland (Available at www.swisstopo.admin.ch).

Pearson F.J., Tournassat C. and Gaucher E.C. (2011) Biogeochemical processes in a clay formation in situ experiment: Part E – Equilibrium controls on chemistry of pore water from the Opalinus Clay, Mont Terri Underground Research Laboratory, Switzerland. *Appl. Geochem*. **26**, 990–1008.

Reynolds R.C. (1985) *A computer program for the calculation of one-dimensional diffraction pattern of mixed-layered clays*. R.C. Reynolds, 8 Brook Rd., Hanover, NH 03755, USA.

Sacchi E., Michelot J.-L. and Pitsch H. (2000) *Porewater extraction from argillaceous rocks for geochemical characterisation*. Nuclear Energy Agency, OECD, Paris.

Seilacher, A., Andalib, F., Dietl, G., and Gocht, H. (1976) Preservational history of compressed Jurassic ammonites from southern Germany. Neu. Jb. Geol. Paläont., Abh. **152**, 307–356.

Tournassat C. and Appelo C.A.J. (2011) Modelling approaches for anion-exclusion in compacted Na-bentonite. *Geochim. Cosmochim. Acta* **75**, 3698–3710.

Tournassat C., Gailhanou H., Crouzet C., Braibant G., Gautier A. and Gaucher E.C. (2009) Cation exchange selectivity coefficient values on smectite and mixed-layer illite/smectite minerals. *Soil Sci. Soc. Am. J*. **73**, 928–942.

Tournassat C., Lerouge C., Blanc P., Brendle J., Greneche J.-M., Touzelet S. and Gaucher E.C. (2008) Cation exchanged Fe(II) and Sr compared to other divalent cations (Ca, Mg) in the Bure Callovian-Oxfordian formation. Implications for porewater composition modelling. *Appl. Geochem*. **23**, 641–654.

Tournassat, C., Gailhanou, H., Crouzet, C., Braibant, G., Gautier, A., Lassin, A., Blanc, P. and Gaucher, E.C. (2007) Two cation exchange models for direct and inverse modelling of solution major cation composition in equilibrium with illite surfaces. *Geochim. Cosmochim. Acta* **71**, 1098–1114.

Tremosa J., Arcos D., Matray J.M., Bensenouci F., Gaucher E.C., Tournassat C. and Hadi J. (2012) Geochemical characterization and modelling of the Toarcian/Domerian

porewater at the Tournemire underground research laboratory. *Appl. Geochem*. **27**, 1417–1431.

Waber H.N., Heidinger M., Lorenz G. and Traber D. (2014) *Hydrochemie und Isotopenhydrogeologie von Tiefengrundwässern in der Nordschweiz und im angrenzenden Süddeutschland*. Nagra Working Report NAB 13-63. Nagra, Wettingen, Switzerland (Available at www.nagra.ch).

Wersin P., Mazurek M., Waber H.N., Mäder U.K., Gimmi T., Rufer D. and De Haller A. (2013) *Rock and porewater characterisation on drillcores from the Schlattingen borehole.* Nagra Arbeitsbericht NAB 12-54, Wettingen, Switzerland (Available at www.nagra.ch).

Figure captions

Fig. 1: Simplified geological profile encountered in the Schlattingen borehole (section above 491 m depth not shown). White sections contain permeable strata, grey shaded units represent aquitards.

Fig. 2: Distribution of the three main mineral fractions for standard samples (classification after Füchtbauer 1988)

Fig. 3: Water-loss (WL) porosity and clay-mineral content vs. depth

Fig. 4: Observed diagenetic minerals on 6 samples (red) and vein minerals on 10 samples (blue) from microscopic analysis as function of depth. cc: calcite; do: dolomite; ank: ankerite; sid: siderite; py: pyrite; Sr-Ba-S: Sr-Ba sulphate; cel: celestite; chl: chlorite; chal: chalcedony; kao: kaolinite; il: illite; phos: phosphorite

Fig. 5: Water-loss porosity as a function of the clay-mineral content

Fig. 6 a) Cl^- and b) SO_4^{2-} concentration of aqueous extracts (mg/kg rock) vs. S/L ratio (g/g); symbols: green – Effingen M. (SLA 734.89), light brown – 'Brown Dogger' (square: SLA 778.70, circle: SLA 823.53), red – Opalinus Clay (SLA 860.77), purple – Lias (SLA 971.89)

Fig. 7: a) Na^+ and b) Ca^{2+} concentration (mg/kg rock); symbols: same as in Fig. 6

Fig. 8: Cation concentrations (meq/kg_{rock}) in Ni-extract vs. S/L ratio

Fig. 9: Ni consumption as proxy for the cation exchange capacity (CEC), sum of cations in the Ni-en extract solutions and calculated CEC from illite, smectite contents (meq/kg_{rock}) versus depth for S/L = 1

Fig. 10: Evolution of the CO_2 partial pressure in the ten gas cells during the solid/gas equilibration time

Fig. 11: Chloride concentrations in squeezed waters, calculated from aqueous extracts (S/L=1), and in a groundwater sample as function of depth; a) concentration in aqueous extracts back-calculated to water-loss porosity; b) concentration in aquoeus extracts back-calculated to a constant anion-accessible porosity fraction of 0.52.

Fig. 12: Anion-accessible porosity fraction derived from chloride data of squeezed samples as function of clay-mineral content (Table 4). Error of anion-accessible porosity was estimated to be 13% based on linear error propagation of analytical errors.

Fig. 13: Sulphate concentrations in squeezed waters, aqueous extracts (back-calculated to water-loss porosity) and the groundwater sample from the 'Brown Dogger' vs depth

Fig. 14: Ratio of exchangable Ca and Na as equivalent fractions as function of depth. Data of aqueous extracts (S/L = 0.1 and S/L = 1.0) calculated with cation exchange model. Measured data from Ni extracts (S/L =1) shown as comparison.

Fig. 15: Schoeller diagram comparing ion compositions from squeezing (circles) with modelled data (lines). Red solid line: case A (base case) ; green dashed line: case B (constant initial SO4/Cl); case C (corrected cation exchange composition); case E (assuming gypsum equilibrium). Case D shows almost identical results as Case A (see text).